HHS Public Access

Author manuscript

Nat Genet. Author manuscript; available in PMC 2022 March 06.

Published in final edited form as:

Nat Genet. 2021 September ; 53(9): 1348–1359. doi:10.1038/s41588-021-00920-0.

Genomic and evolutionary classification of lung cancer in never smokers

A full list of authors and affiliations appears at the end of the article.

Abstract

Lung cancer in never smokers (LCINS) is a common cause of cancer mortality, but its genomic landscape is poorly characterized. Here, high-coverage whole genome sequencing of 232 LCINS showed three subtypes defined by copy number aberrations. The dominant subtype (*'piano'*), rare in lung cancer in smokers, features somatic *UBA1* mutations, germline *AR* variants, and stem cell-like properties, including low mutational burden, high intra-tumor heterogeneity, long telomeres, frequent *KRAS* mutations, and slow growth, as suggested by the occurrence of cancer drivers' progenitor cells many years prior to tumor diagnosis. The other subtypes are characterized by specific amplifications and *EGFR* mutations ('*mezzo-forte*'), and whole genome doubling (*'forte'*). No strong tobacco smoking signatures were detected, even in cases with exposure to second-hand tobacco smoke. Genes within the RTK-RAS pathway had distinct impacts on survival, and five genomic alterations independently doubled mortality. These findings create avenues for personalized treatment in LCINS.

Lung cancer is the leading cause of cancer-related deaths with ~2 million people diagnosed each year[1]. Lung cancers in never smokers (LCINS) account for 10–25% of all lung cancers, with most LCINS being lung adenocarcinomas (LUAD)[2]. Several studies have profiled the genomic landscape of LUAD[3–10] and the rarer carcinoid subtype[11]. Previous LUAD samples were mostly from smokers, primarily subject to whole exome sequencing (WES). The largest moderate- to high-coverage whole genome sequencing (WGS)-based LUAD studies cumulatively total less than 100 LCINS subjects, mostly of Asian ancestry[4,8,10,12–14]. As part of the Sherlock-*Lung* study[15], we evaluated the genomic landscape and mutational processes in 232 treatment-naïve LCINS using high-coverage WGS (tumor: 70.6–141.5×, mean: 85×; normal: 26.2–57.2×, mean: 31.6×) (Supplementary Table 1). Three subtypes based on somatic copy number alterations (SCNAs) were observed, with major genomic differences from LUAD in smokers, and distinct clonal evolutionary patterns affecting diagnosis and possibly survival. Our findings suggest developmental processes and possible novel therapeutic approaches for LCINS.

*Correspondence: landim@mail.nih.gov (Maria Teresa Landi).

Author Contributions

Conceptualization, MTL, TZ; Methodology, TZ, DCW, JS, BZ, NA-P, NL-B, BZ, SHW, YP, HC, TR, DS, DAG, LBA, MTL; Formal Analysis, TZ, NA-P, WZ, PHH, RL, AG, FM, AC, IP, JS, JK, NS, LJK, AMAI, BO, AK, AM, CFK; Laboratory work, AH, NC, JC, KB; Pathology work: MO, SML, MD, PL, PD, JDA; Resources, PJ, YB, PH, DC, ACP, LAM, BEGR, MBS, NEC, ML, SJC; Data Curation, MK, LM, JR; Writing – Original Draft, TZ, MTL; Writing – Review & Editing, DCW, SJC, YB, QL, NR, MG-C, DAG, LBA, NL-B, BZ, JS, TZ, PHH, MTL; Visualization, all authors; Supervision, MTL.

Competing interests

The authors declare no competing interests.

Characteristics of Sherlock-*Lung* Cancer Patients

Fresh frozen tumor tissue and matched germline DNA were obtained from 232 treatment-naïve never smoker lung cancer patients with unknown exposures to lung cancer risk factors, with the exception of second-hand ('passive') tobacco smoking in 27.6% of patients (Methods, Supplementary Table 1). Patients were diagnosed with non-small-cell lung cancer, including 189 adenocarcinomas, 36 carcinoids, and 7 other tumors of various subtypes (Methods). Patients were predominantly of European descent (n=226; 97.4%), with the remainder of Asian (n=4; 1.7%) or African (n=2; 0.9%) ancestry (Supplementary Fig. 1).

Genomic characteristics of LCINS

The median tumor mutational burden (TMB) was 1.1 Mut/Mb (single nucleotide variation (SNV)=1.0; insertions and deletions (indel)=0.06), more than 7-fold lower than in smokers[4] (*P* = 7.0e-73) (Fig. 1). TMB was significantly associated with tumor stage, histology, and age at diagnosis, but not tumor purity (Supplementary Fig. 2).

The major genomic characteristics of LCINS are summarized in Fig. 2 and in the Supplementary Note. Among genes in the RTK-RAS pathway, *EGFR* was the most frequently altered (30.6%), followed by *KRAS* (7.3%), *ALK* (6.0%), *MET* (4.3%), *ERBB2* (3.9%, all indels), *ROS1* (2.6%) and *RET* (1.3%). A strong mutually exclusive distribution was observed across these seven genes, which were altered in total in 54.3% of tumors (Extended Data Fig. 1a). The pattern of genomic alterations was strikingly different between RTK-RAS$^+$ and RTK-RAS$^-$ groups (Extended Data Fig. 1b). The former had significantly higher burden of SNVs/indels, SCNAs, structural variants (SVs), kataegis, whole genome doubling (WGD), and *BRCA2* loss of heterozygosity (LOH), but lower tumor/normal telomere length (T/N TL) ratios. The 49 (21.1%) tumors bearing both TP53 deficiency and activating RTK-RAS mutations had higher TMB, as previously observed[16], and also higher kataegis, WGD, and LOH in genes associated with DNA homologous repair, than tumors with either TP53 deficiency or RTK-RAS alterations alone (Supplementary Fig. 3).

As expected[17], *TP53* mutations were mutually exclusive with *MDM2* amplifications (*P*=0.03; Extended Data Fig. 2a) and tumors with mutations in either gene (25.4% in total) were enriched with genomic alterations including SNVs, SCNAs, SVs, kataegis, WGD, human leukocyte antigen (HLA) LOH and LOH in *BRCA1* (Extended Data Fig. 2b).

SVs were enriched in hotspot regions, including *MDM2*, *TERT*, *6p21*, *MYC*, *CDKN2A*, *NKX2–1*, and *GNAS*, which together contributed 16.7% of SVs (>200 breakpoints within 5Mb window, Extended Data Fig. 3) as observed in multiple tumor types[18]. Known driver fusion oncogene-generating rearrangements were observed in 24 (10.3%) tumors (Supplementary Table 2) and were mutually exclusive with *EGFR* mutations (*P*=1.1e-4). Non-clustered SVs were enriched in TP53-deficient tumors and RTK-RAS+ tumors (Supplementary Fig. 4a-c).

Copy Number Alteration Subtypes

Unsupervised clustering of arm-level SCNAs identified three distinct subtypes, with increasing levels of SCNAs (Fig. 3a). Subtype 1 (49.6% of all tumors) largely lacked SCNAs despite relatively high purity, and included 33 of 36 carcinoids and 78 adenocarcinomas. Subtype 2 (30.2%) was enriched with chromosome arm-level amplifications, primarily of 1q, 5p, 7p, 7q (each with $P<0.001$ subtype 2 vs other subtypes, Fisher's exact test), and 8q (exclusively in subtype 2). Subtype 3 (20.2%) was dominated by WGD. Hereafter we refer to these three subtypes respectively as "*piano*", "*mezzo-forte*" and "*forte*", borrowing the terms from musical dynamics. Combining our copy number profiles with those of LUAD from smokers (n=38)[12], the majority of LUAD from smokers (20/38, 52.6%) fell into the subtype *forte* (P=6.6e-5) (Supplementary Fig. 5a). Focal amplifications of *MDM2* and *EGFR* were significantly less frequent in subtype *piano* than in *forte* and *mezzo-forte* (P=0.001 and P=0.02 respectively, Supplementary Table 3, Supplementary Fig. 5b). Mitochondrial-DNA copy numbers were higher than previously reported in LUAD from smokers (P=0.01)[19] (Supplementary Note, Supplementary Fig. 6a-c). HLA-LOH has been previously identified in nearly 40% of lung cancer cases, particularly squamous cell carcinomas[20]. In our cohort, only 5.2% of tumors (all LUAD, mostly in *forte* and *mezzo-forte*) harbored HLA-LOH (Methods, Supplementary Table 1).

Genomic features across SCNA subtypes

Notably, several other genomic features of LCINS differed between SCNA-defined subtypes. TMB was much lower in the *piano* subtype (0.7 Mut/Mb), particularly in carcinoids (0.4 Mut/Mb), compared to *forte* (1.4 Mut/Mb) and *mezzo-forte* (1.6 Mut/Mb) (P=2.0e-7 and 3.2e-11, respectively) (Fig. 3b).

While 24/25 recurrently mutated genes (Supplementary Table 4, Supplementary Fig. 7) were previously identified as drivers in the TCGA PanCancer cohort[21], many of them had substantial frequency differences from LUAD in smokers and across SCNA subtypes (Extended Data Fig. 4; Fig. 2). For example, *TP53* mutations were most common in *forte* (31.9%, 18.6% and 7.0% for *forte*, *mezzo-forte* and *piano*; P=1.2e-3), while remaining lower than in LUAD from smokers (53.4%)[21]. Further, we identified one likely new driver gene, *UBA1* (6/9 in *piano*), which encodes an E1 ubiquitin conjugating enzyme that acts as one of the main orchestrators of the cellular DNA damage response[22]. All 25 recurrently mutated genes exhibited signals of positive selection[23] (Extended Data Fig. 5).

Over half of the tumors in *mezzo-forte* had *EGFR* mutations (51.4% *vs*. 9.0% in LUAD from smokers), while only 1.4% had *KRAS* mutations (*vs*. 34.0% in LUAD from smokers). Tumors in *piano* were less likely to have TP53 deficiency or aberrations in *EGFR* and other RTK-RAS genes (P=4.4e-6 and 4.3e-7, respectively), with the exception of *KRAS* (76.5% of $KRAS^+$ tumors were in *piano*, P=0.02). While carcinoids in *piano* were enriched (P=7.5e-4) with mutations in chromatin-remodeling genes (e.g., *ARID1A*) as previously observed[11], LUAD in this subtype rarely harbored a known recurrent driver, with the exception of mutations in *NKX2–1* (n=4, only in *piano*), *SETD2* (n=8/10 in *piano*) and *UBA1*. These *piano* tumors exhibited low burden of SNVs/indels, SCNAs, SVs, kataegis,

and WGD, as well as a high T/N TL ratio and subclonal mutation ratio, with carcinoids being exceptionally quiet (Fig. 3b).

The median number of SVs per tumor varied widely between SCNA subtypes, with 73, 63, and 10 in *forte*, *mezzo-forte* and *piano*, respectively, distributed as translocations (52.4%), deletions (32.7%), and tandem duplications (14.5%) (Supplementary Fig. 8). Of note (Extended Data Fig. 4), *RET* fusions were present only in the piano subtype (2.6%).

Rare, predicted deleterious, germline variants were identified[24] (Methods, Supplementary Table 5) recurrently in *CYP21A2*, which encodes the 21-Hydroxylase enzyme involved in the synthesis of cortisol and aldosterone (n=8, 6 with an identical stop-gain variant, more common in *forte* and *mezzo-forte*) and *GLUD2,* which encodes for Glutamate Dehydrogenase 2 in the mitochondria (n=6, identical variant). Among known cancer susceptibility genes, *AR* was the most frequently mutated (n=5, 4 of which in *piano*). Variants in both *CYP21A2* and *AR* suggest a role for hormones in driving LCINS, warranting further investigation. A handful of tumors had germline variants in homologous recombination genes[25], including *BRCA1* (n=3, 2 of which in *piano*), *ATM* (n=2), and *RAD51D* (n=2). Single variants, one per tumor, were identified in *CDK4* in *forte*, *SOS1* in *mezzo-forte*, and *RET* and *MSH6* in *piano*.

Mutational Signatures in LCINS

Mutational signature deconvolution of single base substitutions (SBS) using SigProfiler[26,27] identified 14 previously reported signatures from COSMIC (Supplementary Table 6, Fig. 4, Supplementary Fig. 9). Notably, SBS18, related to damage by reactive oxygen species (ROS)[28], was observed in 46% of samples, particularly in SCNA subtypes *forte* and *mezzo-forte* (59.6% and 67.1%, respectively, P=2.2e-9 in comparison to *piano*). SBS8, linked to nucleotide excision repair deficiency[29] and late replication errors[30], was present in 13% of samples, particularly in carcinoids (30.3%, P=2.7e-4). In the 38 LUAD from PCAWG[12], SBS8 was not identified, indicating possible differences in the etiology of tumors from smokers and never smokers. Signature extraction using indel (ID-83) and double base substitution (DBS-78) profiles[26] identified six ID (ID1, 2, 3, 5, 8, and 9) and four DBS (DBS2, 4, 9, and 11) signatures (Supplementary Fig. 10).

About 58% of samples (n=135) had ≥100 SNVs, mostly subclonal (median fold-change=1.2, interquartile range=1.0–1.5), assigned to APOBEC mutational signatures SBS2 and SBS13 (Supplementary Note, Supplementary Fig. 11a,b), with substantial inter-tumor heterogeneity (Fig. 4). APOBEC mutational loads were verified using P-MACD[31] (Supplementary Note, Supplementary Fig. 11c). APOBEC signatures were dominant (>80%) in 4 hypermutated tumors (TMB>8 Mut/Mb), 1 in *forte* and 3 in *piano*. Significant enrichment of the APOBEC signature was observed in TP53-deficient (P=1.9e-8) and RTK-RAS+ (P=3.5e-8) tumors.

In all tumors, endogenous processes (Supplementary Table 7) predominated over exogenous processes[32] (median cosine similarities of 0.96 and 0.82, respectively, P=4.8e-53, Extended Data Fig. 6). Only a few samples showed higher cosine similarities combining exogenous and endogenous signatures in comparison with endogenous signatures alone (Supplementary

Fig. 12), particularly 6 tumors (4 in *piano*) with a signature of nitrated polycyclic aromatic hydrocarbons (Nitro-PAH), 1,8 dinitropyrene [DNP])[32], contributing 18.7% of SNVs on average in these samples. No additional dominant or recurrent genomic events were apparent in these tumors (Supplementary Fig. 13). Nitro-PAHs derive mostly from diesel exhaust and are associated with cancer risk[33].

The mutational signature associated with direct exposure to tobacco smoking (SBS4) was not observed, even in 62 cases with reported exposure to second-hand tobacco smoking ("passive smoking") (Fig. 4). Our simulations demonstrated that signature SBS4, if present, is below the detection threshold of 15% of somatic mutations (Supplementary Note, Supplementary Fig. 14). The lack of passive smoking signatures was not explained by tumor purity differences between passive and non-passive smokers (P=0.39, Fig. 5a), and was confirmed by measuring alkylation-induced mutagenesis[34] (Supplementary Note, Fig. 5b). Directly comparing the mutational patterns in passive *versus* non-passive smokers, we found strong similarities between the two groups (Fig. 5c-e) (Q>0.05 for all SBS, DBS and ID signatures), even comparing highly and lowly exposed subjects (Methods, Supplementary Fig. 15, Supplementary Table 8) or comparing strand asymmetries for mutation types or SBS signatures (Supplementary Fig. 16-17). Of note, tumors from passive smokers had shorter telomere length (P=0.005, Supplementary Fig. 18).

Genomic Instability

Overall, 36.2% of tumors had WGD, with much higher prevalence in the *forte* subtype (95.7%, *vs.* 41.4% and 8.7% in *mezzo-forte* and *piano*, respectively) (Extended Data Fig. 4). Similarly, the proportion of the genome affected by SCNAs was much lower in *piano* than *forte* or *mezzo-forte* tumors (P=6.8e-35; Supplementary Fig. 19).

Kataegis was identified in 49.6% of tumors, with an average of 4 events per sample (range: 1–55), rarely in *piano* tumors (29.6%, *versus* 68.1% and 70%, in *forte* and *mezzo-forte*, respectively; P=1.3e-9). As expected, mutations within kataegis events had APOBEC-related signatures[26] in both APOBEC3A-like and APOBEC3B-like tumors[35] (Supplementary Note, Supplementary Fig. 20). Kataegis frequently occurred within the *MDM2* locus (P=1.3e-15) and often co-localized with SVs (Supplementary Fig. 21).

We estimated telomere length (TL) using two previously published methods[36,37], with comparable results, confirming an inverse correlation with age (r=−0.14, P=0.04), and no association with tumor purity (Supplementary Fig. 22). Notably, tumor TL in LUAD of LCINS was significantly longer than that observed in LUAD of smokers[36] (6.4 Kb, 95% confidence intervals [CI]: 5.3–7.6 Kb, P=7.1e-11, Extended Data Fig. 7a, Supplementary Fig. 23). Losses of 9q, 9p, and 22q, and HLA LOH were significantly associated with TL shortening (two-sided t-test; $Q < 0.05$), and were most frequent in *forte* and *mezzo-forte* (Extended Data Fig. 7b,c). While tumors in *forte* had significantly shorter telomeres (mean T/N TL ratio 0.9, P=0.01, t-test), *mezzo-forte* tumors displayed no significant difference, and *piano* had significantly longer telomeres than their matched normal tissues (mean T/N TL ratio 1.1, P=4.7e-3).

Approximately 16.0% (n=37) of tumors had a high HRDetect score[25,38,39] (>0.7), with genomic aberrations predictive of Homologous Repair Deficiency (HRD) (Extended Data Fig. 8), particularly in *forte* and *mezzo-forte* (*P*=1.4e-3 versus *piano*) (Fig. 3b). Biallelic loss of *ATM* in one tumor and monoallelic loss of HRD-associated genes in 42% of tumors had higher HRDetect scores (Extended Data Fig. 9).

The Evolutionary History of LCINS

We reconstructed the likely order of acquisition of recurrent genomic aberrations, including SCNAs, WGD, and common cancer driver genes within each of the SCNA subtypes in LUAD (Methods, Fig. 6). In all three subtypes, mutations in driver genes *TP53*, *RBM10*, *KRAS* or *EGFR* were generally early events, occurring prior to both WGD and most other SCNAs. Two exceptions in *mezzo-forte* were the earlier occurrences of LOH on 17p targeting *TP53* and LOH on 3p12.2, likely targeting transcription factor *ZNF717*, suggesting that these events are also early drivers of *mezzo-forte* tumors. Whereas putative copy number drivers in *mezzo-forte* were balanced between gains and LOH, *forte* was dominated by LOH events. Compared to *mezzo-forte*, WGD generally occurred after other key SCNAs in *forte*. Early events in *piano* included mutations in *SETD2,* LOH of 8p and 17p, and focal gain at 3p12.2, and at 2p11.2 involving the immunoglobulin gene *IGKV1–5*.

Using the proportion of mutations on ≥2 chromosome copies allows for the relative timing of clonal copy number gains and copy-neutral LOH (CN-LOH)[40,41]. Gains of 5q, 16p, 1p, and 14q occurred early during tumor development, whereas gain of 7q and CN-LOH events occurred relatively late (Supplementary Fig. 24a). Reversing this method to time driver mutations relative to clonal gains or CN-LOH identified that mutations in *EGFR*, *MET*, *KRAS*, *ERBB2*, *TP53*, and *UBA1* generally occurred before the corresponding copy number gain (Supplementary Fig. 24b). In contrast, mutations in *PIK3CA* and *SFTPB* occurred after gain events.

We adopted a previously validated model[42] using the clock-like mutations (CpG>TpG in an NpCpG context) to time the appearance of the most recent common ancestor (MRCA) of all tumor cells. We used an estimated acceleration rate of 1×, given the low mutational burden and the paucity of exogenous mutational signatures in LCINS. The MRCA, by definition, possesses all driver mutations for tumorigenesis. Grouping tumors according to common driver events (>3% frequency) (Fig. 7a) enables the estimation of the occurrence of these events in an individual's lifetime. For example, in tumors with *EGFR* mutations the MRCA was estimated to appear at 61 years of age, but the tumors became clinically evident a median of 8 years later. There were substantial latency differences across tumors with different drivers. For example, in tumors harboring *ERBB2*, *CDKN2A*, or *TP53* mutations, or *NKX2–1*, *STK11*, or chr22q SCNAs, the MRCA appeared more than a decade prior to clinical diagnosis. In contrast, tumors with *MDM2* amplifications, or *MET*, *RBM10, HUWEI1* or *KRAS* mutations, had much shorter latency. Notably, tumors in *piano* had significantly longer latency (median: 9.10 years) than *forte* (median: 0.08 years) and *mezzo-forte* (median: 0.28 years) (*P* = 8.3e-4, Fig. 7b), suggesting a large amount of time passed between the last clonal sweep and diagnosis, during which mutations continued to accumulate. This observation was robust to assumed acceleration parameter values between

1× and 20× (Supplementary Fig. 25). We also observed a lower age of appearance of the MRCA in *piano* (median: 60.4 years), particularly the *piano* with carcinoid histology (median: 55.0 years) compared to *forte* (median: 63 years) (all *piano*: $P = 0.038$; *piano* carcinoids: $P = 0.062$, Fig. 7c), which requires further confirmation in larger future studies.

Impact of molecular pathways on survival

Cases with *TP53* mutation or *MDM2* amplifications had poor survival (hazard ratio [HR]=2.9, 95% confidence interval CI=1.6–5.2, *P*=4.5e-4; Supplementary Fig. 26a,b), as previously reported in LCINS[43] and NSCLC[44], with a suggestive stronger impact of *TP53* mutations compared to *MDM2* amplifications (Fig. 8a). Similarly, *EGFR* mutation, *CHEK2* LOH, 22q loss, and 15q loss were associated with poor survival (Fig. 8b-e). A risk score calculated as the mutational burden of these five independent genomic alterations (Fig. 8f) showed an increment of mortality risk for each genomic alteration of approximately 1.9 (CI=1.5–2.4, *P*=3.7e-7).

Interestingly, no significant association was found between RTK-RAS status and overall survival (Supplementary Fig. 26c). However, there were strong differences in clinical association patterns across different genes in the pathway (Fig. 8b). Patients with *ERBB2* mutations had poor overall survival (HR=5.7, CI=1.6–20.4, *P*=7.2e-3), although >50% of ERBB2$^+$ tumors (4/7) also harbored *TP53* alterations, requiring further confirmation in ERBB2$^+$/TP53$^-$ tumors. *KRAS* mutations and *ALK* fusions were also associated with poor survival, but not significantly. In contrast, patients with *MET*-altered tumors had better overall survival than the RTK-RAS$^-$ group. The small number of patients with both TP53-deficient and RTK-RAS$^-$ tumors (n=8) had poorer survival (HR=5.3, CI=1.8–15.2, *P*=2.0e-3; Supplementary Fig. 26d).

Patients with *piano* tumors had overall better survival (HR=0.52, CI=0.3–0.9, *P*=0.03), particularly patients with carcinoids (HR=0.24, CI=0.06–1.0, *P*=0.05), as did patients with *SETD2* positive tumors (HR=0.13, CI=0.02–1, *P*=0.05) (Supplementary Fig. 26e-g).

Discussion

WGS of 232 LCINS samples revealed three subtypes based on SCNAs and profound differences from adenocarcinomas in smokers. Whereas WGD is observed in over 60% of LUAD in smokers[42,45] and is considered to be a major driver of aggressive lung adenocarcinomas[46,47], it occurs in 36% of LCINS overall, but in 95.7% of the *forte* subtype. While *mezzo-forte* is enriched for specific chromosomal arm-level amplifications and has frequent *EGFR* mutations, tumors in the quiet *piano* have low mutation burden, infrequent WGD, small numbers of known drivers, and a larger proportion of subclonal mutations indicative of extensive intra-tumor heterogeneity.

F*orte* tumors and tumors from passive smokers had shorter telomeres than their matched normal samples, while *piano* had longer telomeres, suggesting fewer cell divisions. *TERT* was amplified in only 11.6% tumors and had promoter mutations in only 0.9%, and they were rarely in *piano*, excluding a major role for TERT reactivation in TL elongation.

Notably, we found no major difference between passive and non-passive smokers for mutational signatures or mutation types, while we observed a few tumors with diesel exhaust signatures. Simulation studies showed that smoking-related mutations in the 62 tumors from passive smokers had to be below the detection threshold of 15%. It is possible that SBS4 is present in some passive smokers below this mutation threshold. Second-hand tobacco smoke has been causally linked to lung cancer[48], but it is a weak carcinogen compared to active smoking[48,49] and may also act through alternative tumorigenic processes and selective constraints[50]. Larger studies including highly exposed cases and *in vitro* or animal models are needed to definitively characterize the tumors arising from these exposures.

The long telomeres, low growth rate suggested by the occurrence of the MRCA approximately a decade prior to tumor diagnosis, scarcity and heterogeneity of driver mutations, low mutation rate, high ITH, and paucity of SBS18 indicating low ROS activity[51], are all consistent with *piano* tumors being derived from adult stem cells that have exited their quiescent state[52,53]. Driver genes specifically mutated in *piano* also suggest stem-like features. Oncogenic mutations in *KRAS*, the most frequently mutated driver gene in *piano*, have been shown to induce proliferation of bronchioalveolar stem cells, giving rise to lung adenocarcinoma[54]. Similarly, KRAS[55,56] and UBA1[57] have important regulatory roles in hematopoietic and pluripotent stem cells. The presence of fusions and germline variants in *RET* (as well as mutations in *NKX2*, a regulator of *RET*[58]) uniquely in *piano* suggests a role for RET in these tumors. RET expression and activity are enriched in human hematopoietic stem cells (HSCs)[59] and are involved in murine HSC regulation[60]. Notably, *ARID1A* is essential for telomere cohesion[61], deleting *Arid1a* in mice greatly enhances the ability to regenerate organ tissues[62–64], and *ARID1A* depletion in humans promotes cells to enter the cell cycle[65]. Mutations in *ARID1A*, as well as *NOTCH1*, another gene whose signaling has a role in stem cell expansion and progenitor cell survival[66], have been found in normal and near-normal bronchial epithelial cells from former smokers[67], which are also characterized by long telomeres and polyclonal origins. Notably, alterations in *KRAS, UBA1, RET* and *ARID1A* were mutually exclusive in *piano*. Hypothetically, mutations in *NOTCH1, ARID1A* or other genes with similar function could promote exit from a quiescent cell state, resulting in high ITH, and could drive some of the tumors with no detected known cancer driver gene mutations or fusions. Carcinoids and LUAD in *piano* would then represent tumors diagnosed prior to acquisition of a dominant clone. Using RNA sequencing for an orthogonal assessment of stemness and cell of origin (Methods, Supplementary Note), we found that both a “development score”, incorporating expression of the *SOX2*, *SOX9*, and *HMGA2* genes[68–70], and a marker of basal cells suggesting lineage infidelity[71] were higher in *piano* (Supplementary Fig. 27), consistent with *piano* representing a stem cell-like state. Larger studies are needed to verify the WGS-based stemness hypothesis, possibly using single-cell RNA sequencing and methylome analyses, particularly in tumors with no apparent drivers.

The founder cells of *piano* appear around a decade before diagnosis and provide an optimal time window for early detection. In contrast, driver gene mutations and WGD or gross SCNAs in the *forte* and *mezzo-forte* are generally clonal, with later onset followed by rapid expansion of a single ancestral cell. Their clonal nature could facilitate identification with a single biopsy and successful treatment.

Currently, treatments targeting the most recurrent genomic alterations in *forte* and *mezzo-forte* are available or are under investigation in clinical trials, namely for TP53[72] or MDM2-TP53 interaction[73], as well as for mutations in *EGFR* or *ERBB2*[74–77], genes that conveyed the poorest survival among the RTK-RAS pathway, and even for tumors with both TP53 deficiency and RTK-RAS mutations (21% of our tumors)[78]. Together with *TP53* and *EGFR* alterations, tumors with loss of chromosome 22q, 15q or *CHEK2* LOH were frequently identified, particularly in *forte*. A 2-fold higher mortality risk was estimated for each of these 5 independent genomic alterations, suggesting that compounds targeting bystander genes that are deleted together with tumor suppressor genes in chromosome arm losses (collateral lethality)[79,80] should be explored in these subtypes. Moreover, >15% of tumors had LOH of an HRD associated gene. Targeting these genes could be a promising therapeutic option to explore. Moreover, mutations in HRD associated genes could act as predictors of immune checkpoint inhibitor response[81], broadening the options for treatment for this subgroup. In contrast, *piano* has a scarcity of driver mutations, offering limited targets for therapeutic intervention. Furthermore, due to low TMB[82–84] and HLA-LOH[20], these patients may not benefit from immunotherapy. However, targeting KRAS[85] and stem cell-associated signaling pathways[51,86], or regulating the stem cell microenvironment[87], are promising for this subtype.

Methods

A detailed description of the methods used in this paper and many additional results are described in the Supplementary Note. Here, we summarize the key aspects of the analysis.

Ethics declarations

Since NCI only received de-identified samples and data from collaborating centers, had no direct contact or interaction with study subjects, and did not use or generate identifiable private information, Sherlock-*Lung* has been determined to constitute “Not Human Subject Research (NHSR)” based on the Federal Common Rule (45 CFR 46; eCFR.gov).

Collection of Lung Cancer Samples

Fresh frozen tumor tissue and matched germline DNA from whole blood samples or fresh frozen normal lung tissue sampled ~3 cm from the tumor were obtained from 256 treatment-naïve lung cancer patients from five institutions/centers (Supplementary Note). Among the 256 samples, 20 were excluded after quality check and four were excluded based on mutational signatures analysis (Supplementary Note). The resulting 232 samples and the associated demographic and clinical data were included in the final analysis. For these 232 subjects, the mean age at lung cancer diagnosis was 64.8 years (range: 21–86); 75.4% of patients were female. To confirm the ancestry of these patients, we estimated the admixture proportions based on WGS data using the fastNGSadmix[88] tool.

Of the 232 tumors, 189 were adenocarcinomas, 36 carcinoids, 5 sarcomatoid carcinomas or undifferentiated non-small cell carcinomas with sarcomatoid features, and 2 squamous cell carcinomas. Three pathologists reviewed the histological diagnoses. Histological images can be found here: https://episphere.github.io/svs. All 232 matched tumor and germline

samples underwent DNA whole genome sequencing. Of these, 35 (all adenocarcinomas) also underwent RNA sequencing.

Genome-Wide Somatic Variant Calling

The analysis-ready BAM files were processed using four different algorithms, including MuTect[89], MuTect2, Strelka (v2.9.0)[90], and TNscope[91]. To improve the performance of the variant calling, we used Sentieon's genomics package (v201808.03) to run MuTect, MuTect2 and TNscope. Only those SNVs that passed calling by a minimum of three algorithms were kept. To reduce false positive calling, we applied an in-house filtering script (https://github.com/xtmgah/Sherlock-Lung) similar to our previous publication[92]. To summarize, variant calling was considered only at the genome positions with 1) read depth >12 in tumor and >6 in normal samples; and 2) variant read count >5 in tumor and VAF <0.02 in normal samples. To remove possible germline variants from the called somatic variants, somatic variants were filtered against the dbSNP138, 1000 genomes (phase 3 v5), ExAC (v0.3.1), gnomAD (v2.1.1)[93] database, and an in-house Italian germline variant database from EAGLE WES study (dbGAP access ID phs002496.v1.p1) for commonly occurring SNPs (somatic variant frequency<0.001). The filtered variants were annotated with Oncotator (v1.9.1.0)[94] and ANNOVAR[95]. For the indel calling, only variants called by three algorithms were kept (MuTect2, TNscope, and Strelka). UPS-indel[96] algorithm was used to compare and combine different indel call sets. Similar filtering steps as those used for SNV calling were also applied to indel calling. The final set of indels were left normalized (left aligned and trimmed) for the downstream analysis. Clustering of subclonal somatic mutations was analyzed using a Bayesian Dirichlet Process (DPClust) as previously described[92,97,98]. Further details are available in the Supplementary Note.

Germline Variant Calling

Final BAM files from paired normal samples were used to call germline variants using the GATK Haplotyper algorithm in Sentieon's genomics package. Default parameters or suggested input files, such as the most recent dbSNP VCF file were applied. The final joint callings from all normal samples were generated and annotated with ANNOVAR[95]. Strict filtering criteria were used to identify the potential pathogenic variants: 1) Minor allele frequencies <0.05% in the GnomAD non-cancer and non-finnish European ancestry dataset (v2.1.1); 2) Estimated CharGer score >4 to include the pathogenic or likely-pathogenic variants based on the CharGer algorithm (version 0.5.2)[99]. The default parameters for CharGer were used and the most damaging interpretation from ClinVar[100], excluding OMIM and genereview as submitters, was used for annotation; 3) Variants predicted to have 'silent' functional activity were removed, including variants in the UTR, upstream or intron regions. All the final germline variants have been manually inspected through IGV and the suspicious variants have been removed.

Driver Gene Discovery

The IntOGen pipeline[23], which combines seven state-of-the-art computational methods, was employed to detect signals of positive selection in the mutational pattern of genes across the cohort. Default parameters were used, and in the post-processing phase, the gene *CSMD3* was filtered out based on warnings provided by the pipeline. The 25 genes identified as

drivers in the cohort were classified according to their mode of action in tumorigenesis (i.e., tumor suppressor genes or oncogenes) based on the relationship between the excess of observed non-synonymous and truncating mutations computed by dNdScv[101] and their annotations in the Cancer Gene Census (CGC). In the case of *UBA1*, only the excess values were used. Genes with conflicting computed and annotated mode of action are labeled ambiguous. To identify potential driver mutations across the 24 cancer driver genes annotated in the CGC, we used boostDM gene-tumor type specific (LUAD) or more general models depending on their availability and accuracy[102].

Somatic Copy Number Alterations (SCNA) Analysis

We used the updated Battenberg (v2.2.8) algorithm[98] to estimate the clonality of each segmentation, tumor purity and ploidy (Supplementary Note). Unsupervised clustering of copy number profiles including both major clone and subclone segmentations were generated based on relative copy number log2 (copy number/Tumor_Ploidy) using the euclidean distance and Ward's method. Recurrent copy number alterations from WGS at a gene level were identified using GISTIC 2.0[103] based on the major clonal copy number for each segmentation (Supplementary Note).

Whole Genome Doubling Identification

Multiple methods were used to determine the genome doubling status for each tumor. First, tumors were considered to have undergone WGD if greater than 50% of their autosomal genome had a major copy number (MCN) (i.e., the more frequent allele in a given segment) >=2[46]. Also, the number of chromosomes with 50% of the segment with MCN>=2 had to be greater than 11. Next, we applied a modified version of the published WGD algorithm[104], where a *p*-value was obtained using 10,000 simulations with observed probabilities of copy number events. For samples with ploidy ≤3 and ploidy=4, *p*-value thresholds of 0.001 and 0.05 were used, respectively. All samples were classified as genome doubled if the ploidy exceeded 4. Tumors were determined to have undergone WGD if the tumors met the criteria for WGD for both methods. Finally, to improve the WGD calling, we manually checked the Battenberg CNA profile to resolve tumors with ambiguous WGD calling (e.g., MCN close to 0.5), evaluating features such as presence of multiple copy losses after WGD (total copy of 3) and/or LOH events having 2:0 copy number state. For the chronological reconstruction of genomic aberrations, we limited the WGD samples with average ploidy > 3.

Structural Variants Calling and Clustering

The Meerkat algorithm[105] was used to call somatic SVs and estimate the corresponding genomic positions of breakpoints (Supplementary Note). The parameters were selected based on the sequencing depth for both tumor and normal tissue samples and the library insert size as in a previous publication[92]. Driver oncogenic fusions were selected from SVs based on the driver gene list[21] and an oncogenic fusion list previously reported in LUAD[8]. We selected the fusions with the following SV features in Meerkat output: "gene-gene", "head-tail" and "in_frame" or "out_of_frame". All driver oncogenic fusions in our study were reported with the same partners and no other new recurrent oncogenic fusion was found.

We used the algorithm developed by Li *et al.*[106] to cluster the SVs in each sample. The algorithm groups the structural variants into clusters based on the proximity of breakpoints, the number of events in that cluster regions and the size distribution of those events. A cluster contains structural variants that have arisen from the same event and are significantly closer than expected by chance, given the orientation and the number of SVs in that patient. In addition, to visualize the hotspots of breakpoints, we counted the number of breakpoints across the whole genome using a 5 Mb window. A similar approach was also applied to visualize the kataegis hotspots.

Telomere Length Estimation

We estimated telomere length (TL) in kb using TelSeq[107]. We used 7 as the threshold for the number of TTAGGG/CCCTAA repeats in a read for the read to be considered telomeric. TelSeq calculation was done individually for each read group within a sample, and the total number of reads in each read group was used as weight to calculate the average TL for each sample. To validate the estimation of telomere length by TelSeq, telomere content was quantified using TelomereHunter[37] using ten telomere variant repeats including TCAGGG, TGAGGG, TTGGGG, TTCGGG, TTTGGG, ATAGGG, CATGGG, CTAGGG, GTAGGG and TAAGGG.

To compare telomere length in Sherlock-*Lung* with previous studies, we collected the telomere length estimation from the same algorithms across the TCGA cohort and applied the same linear mix model to predict the mean telomere length as described by Barthel *et al.*[36].

Mutational Signature Analysis

Mutational signature analysis was analyzed by the updated computational framework SigProfiler[26,108]. SigProfilerExtractor with default parameters was used to perform both *de-novo* extraction and decomposition to known global Cosmic mutation signatures (v3). Mutation probabilities for each mutation type in each sample were generated for grouping samples based on different genomic features. Hierarchical clustering of contribution of mutational signatures was performed using “euclidean” distance and Ward’s minimum variance clustering method.

To investigate the endogenous and exogenous mutational processes in our Sherlock-*lung* study, we collected four mutational signature sets according to the likely etiologies, including 65 Cosmic SBS mutational signatures, 22 Cosmic SBS endogenous signatures, 53 environmental mutagens signatures[32] and 75 combined endogenous and exogenous mutational signatures (See Supplementary Table 7 for the included signatures). We then performed SBS mutational signature analyses as described above. To maximally deconvolute all mutations to these global signatures in SigProfilerExtractor, we decreased the cosine similarity threshold for *de novo* mutational signatures until no new mutational signature was found. Among these 4 mutational signature sets, we compared the cosine similarity between the reconstructed mutational profiles to the original mutational profiles for each sample.

Analysis of Passive Smoking

To investigate tumor mutational patterns between passive smokers and non-passive smokers, we first excluded 4 hypermutated tumors (2 from passive smokers, 1 from a non-passive smoker, and 1 with unknown passive smoking exposure) driven by APOBEC mutagenesis (TMB>8 Mut/Mb). We then compared each mutation type among SBS, DBS and ID between passive and non-passive smokers using the Mann-Whitney U test followed by multiple testing correction using the Benjamini & Hochberg method. To quantify and visualize differences in the overall mutational patterns between passive and non-passive smokers, we combined all mutations in each tumor group into a single profile and estimated their cosine similarity and residual sum of squares (RSS). As a sensitivity analysis, we replicated these analyses within samples from two studies (EAGLE and Yale) with high quality passive smoking exposure data. The EAGLE study had details on exposure during childhood, during adulthood at home, and during adulthood at work. Thus, we created a score from the highest exposure ("1": during all three periods) to the lowest ("4": only one exposure setting during adulthood). We then extracted the mutational patterns across the groups and estimated the cosine similarity of the two extremes (1 and 4).

Homologous Recombination Deficiency by HRDetect

We applied HRDetect to assess the homologous recombination deficiency (HRD) as described in previous studies[25,38,39]. Mutations including SNVs and Indels, Battenberg segmentation profile, SVs, and tumor purity and ploidy were included for HRDetect. HRDetect scores were computed by aggregating six features associated with HRD including SNV signature 3, SNV signature 8, SV signature 3, SV signature 5, HRD index from copy number profile, and the fraction of deletions with microhomology. All the features were normalized and log transformed. A logistic model was used to predict the HRDetect scores using previously trained data[38].

Assessment of Loss of Heterozygosity

Loss of heterozygosity in human leukocyte antigen (LOH HLA) was identified by the LOHHLA algorithm[20]. Patient-specific HLA genotypes were inferred by POLYSOLVER[109] based on the normal samples. Then, tumor and normal BAM files, HLA calls, HLA fasta file, and tumor purity and ploidy were used as input to LOHHLA. A copy number < 0.5 is classified as subject to loss, and thereby indicative of LOH. Allelic imbalance is determined if P <0.01 using the paired t-test between the two distributions.

LOH analysis for HRD genes was based on the overlapping gene location with copy number profile by Battenberg. LOH segmentation was called if the clonal minor copy number was 0. The HRD gene list was based on a previous publication[25].

Prediction of Chronological Timing

We adopted the approach from PCAWG[42] to estimate the elapsed time between the appearance of the MRCA and the last observable subclone in our *Sherlock*-lung study. Briefly, the number of clock-like CpG>TpG mutations in an NpCpG context was counted for all tumors, accounting for tumor ploidy as well as clonal and subclonal mutations. Tumors with no age information, insufficient number of clonal and subclonal clock-like

mutations (<50 mutations/sample) to estimate mutation rate, abnormal mutation rate, or high fraction of APOBEC-associated mutations (SBS2 and SBS13 fraction >70%) were excluded from the analysis as previously advocated [8,42], leaving 153 samples for this analysis. The latency of the MRCA was estimated for each tumor, adopting an estimated tumor acceleration rate of 1×. We subtracted the estimated latency from the age at diagnosis to obtain the real-time age at which MRCA likely emerged, grouping tumors by the presence of specific genomic alterations or features with >3% frequency (such as SCNA subtypes; groups with RTK-RAS alterations, TP53 deficiency, *ALK* fusions, and *ARID1A* mutations, etc.). Significant differences between subgroups were assessed using Wilcoxon rank-sum test.

Timing Model of Ordering Events

Mutational drivers and CNAs were simultaneously incorporated into the timing model based on the clonality of the events. For CNAs, Battenberg copy number calls were used to assign clonality of CNAs (whether cancer cell fraction (CCF)=1 or <1), describe the type of CNA (i.e. gain, LOH and HD) and whether WGD has occurred in the overall copy number profile. To include only recurrent regions, first, CNA events of each type were piled up across all samples along the chromosomes to get the frequency landscape of each CNA type based on all observed breakpoints. Next, a permutation test (N=1,000) followed by FDR-based multiple testing correction was undertaken to identify regions that were significantly enriched above the random background copy change rate. The enriched regions that encompassed the HLA region (6p21), or specific to telomeric ends or present as a singleton were excluded. For each mutational driver (with ≥ 5% recurrence), CCF of each variant was estimated by adjusting VAF according to the CNA status of the locus and purity of the tumor sample as previously described[110]. Variants were then classified as clonal (CCF=1) and subclonal (CCF <1) using DPClust. All events were combined per sample and ordered based on CCF. Where more than one tree could be inferred based on subclonal events, all possible trees were generated and randomly chosen in each iteration of ordering events. To time the events based on the entire dataset, events were ordered based on clonality (randomized clonal events followed by a sampled tree of subclonal events) in each sample. To classify events with respect to WGD, we used the estimated number of chromosomes bearing the mutation (NCBM) and major/minor copy number status to call pre-WGD and post-WGD mutations and CNA respectively. The Plackett-Luce model[111,112] for ordering partial rankings was implemented (https://github.com/hturner/PlackettLuce) to infer the order of events based on the ordering matrix of the entire dataset while allowing for unobserved events. This analysis was undertaken for 1,000 iterations to obtain the 95% confidence interval of the timing estimate of each event. We repeated this analysis across the three subtypes of tumors based on SCNA clusters (*forte*, *mezzo-forte*, and *piano*).

Statistical and Survival Analysis

All statistical analyses were performed using the R software (https://www.r-project.org/). To investigate the functional relevance of potential driver mutations of each pair of genes, we performed mutual exclusivity analysis and co-occurrence analysis using two-sided Fisher's exact test. *P* values less than 0.05 were considered as statistically significant. If multiple testing was required, we applied the false discovery rate (FDR) correction based on the

Benjamini & Hochberg method. For survival analyses, a proportional hazards model was used to investigate the associations between genomic features and overall survival, adjusting for age at diagnosis, gender, and stage. The multiple testing correction for survival analysis was performed based on 33 different genomic alteration events with at least 5% frequency including mutations, focal SCNA, arm-level SCNA, and gene fusions. Genomic alterations were identified as significant if $Q<0.1$. A risk score was calculated as the mutational burden of these significant independent genomic alterations and we then performed association between risk score and overall survival using the same method.

Data Availability

232 normal and tumor paired raw data (BAM files) of the whole genome sequencing datasets have been deposited in dbGaP with accession number: **phs001697.v1.p1**. Researchers will need to obtain dbGaP authorization to download these data. RNA-seq raw data (FASTQ files) have been submitted to NCBI GEO database with access number **GSE171415**. Germline variant dataset from EAGLE whole exome sequencing study can be access in dbGaP with access number **phs002496.v1.p1**. In addition, histological images of these tumors can be found at https://episphere.github.io/svs. Public datasets were used in this study including: gnomAD (v2.1.1)/ExAC (v0.3.1) (https://gnomad.broadinstitute.org/), 1000 genomes (phase 3 v5, https://www.internationalgenome.org/) and dbSNP (v138, https://www.ncbi.nlm.nih.gov/snp/).

Code Availability

The code for whole genome sequencing subclonal copy number caller can be found at https://github.com/Wedge-lab/battenberg (v2.2.8). The code for somatic mutation filtering can be found at https://github.com/xtmgah/Sherlock-Lung. The code for Dirichlet Process based methods for subclonal reconstruction of tumors can be found at https://github.com/Wedge-lab/dpclust (v2.2.8). The code for mutational signature analysis can be found at https://pypi.org/project/sigproextractor/ (SigProfilerExtractor, v0.0.5.77). The code for inferring the order of genomic events can be found at https://github.com/hturner/PlackettLuce (v0.2–2). The code for chronological timing analysis can be found at https://gerstung-lab.github.io/PCAWG-11/. The code for P-MACD (Pattern of Mutagenesis by APOBEC Cytidine Deaminases) can be found at https://github.com/NIEHS/P-MACD.

Extended Data

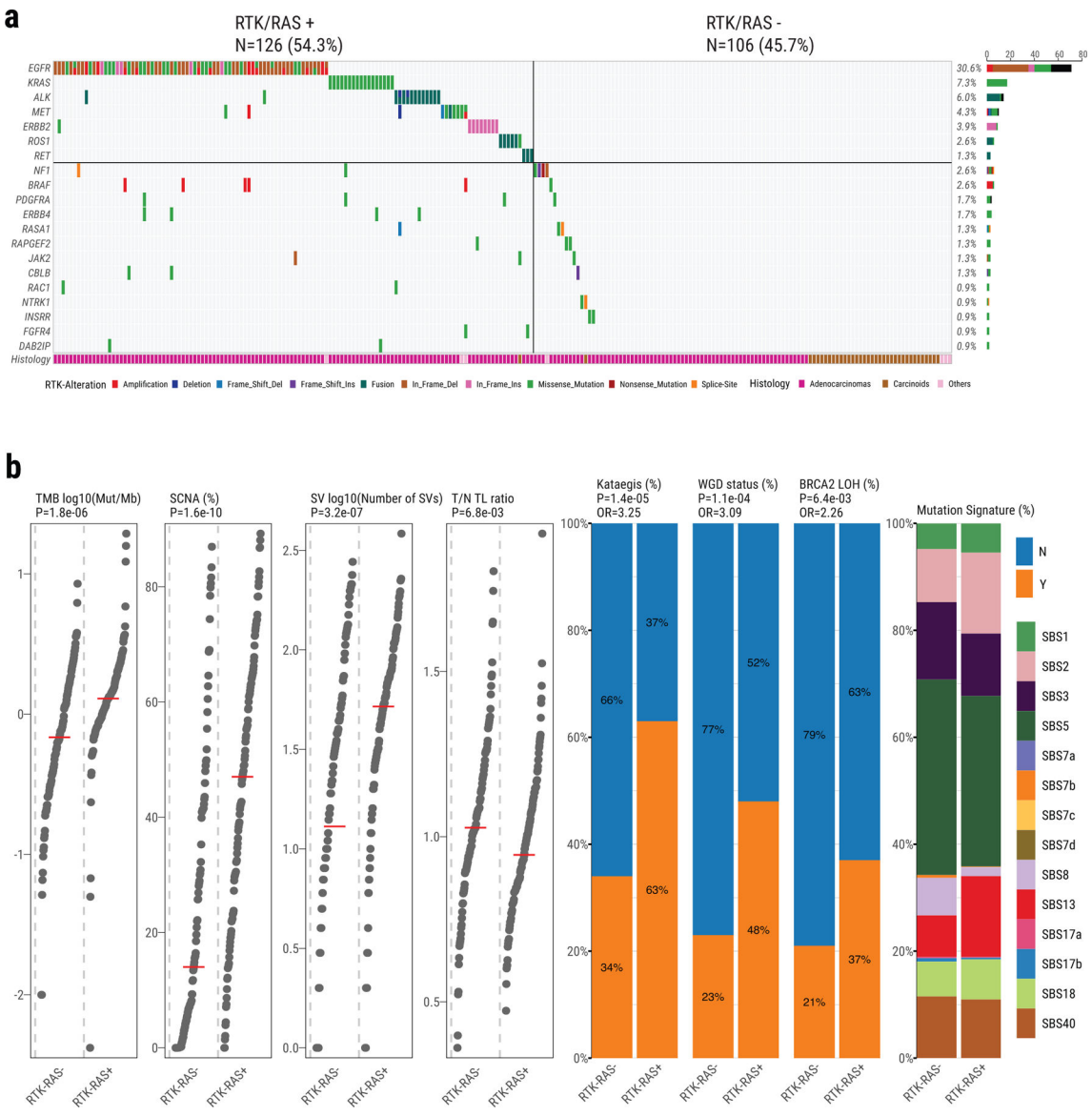

Extended Data Fig. 1. Genomic alterations of RTK-RAS pathway in Sherlock-*Lung*.

a, Oncoplot showing mutual exclusivity of genes within the RTK-RAS pathway, which were used to define the RTK-RAS status. The bottom bar shows tumor histological types. **b**, Comparison of genomic features between RTK-RAS negative and positive tumors. Left four panels: tumor mutational burden, percentage of genome with SCNAs, SV burden and T/N TL ratio. P-values are calculated using the two-sided Mann-Whitney U test; Middle three panels: enrichments for Kataegis events, WGD events, and *BRCA2* LOH. *P*-values and *OR* are calculated using Fisher's exact test (two-sided); Right panel: Contributions of each SBS signature.

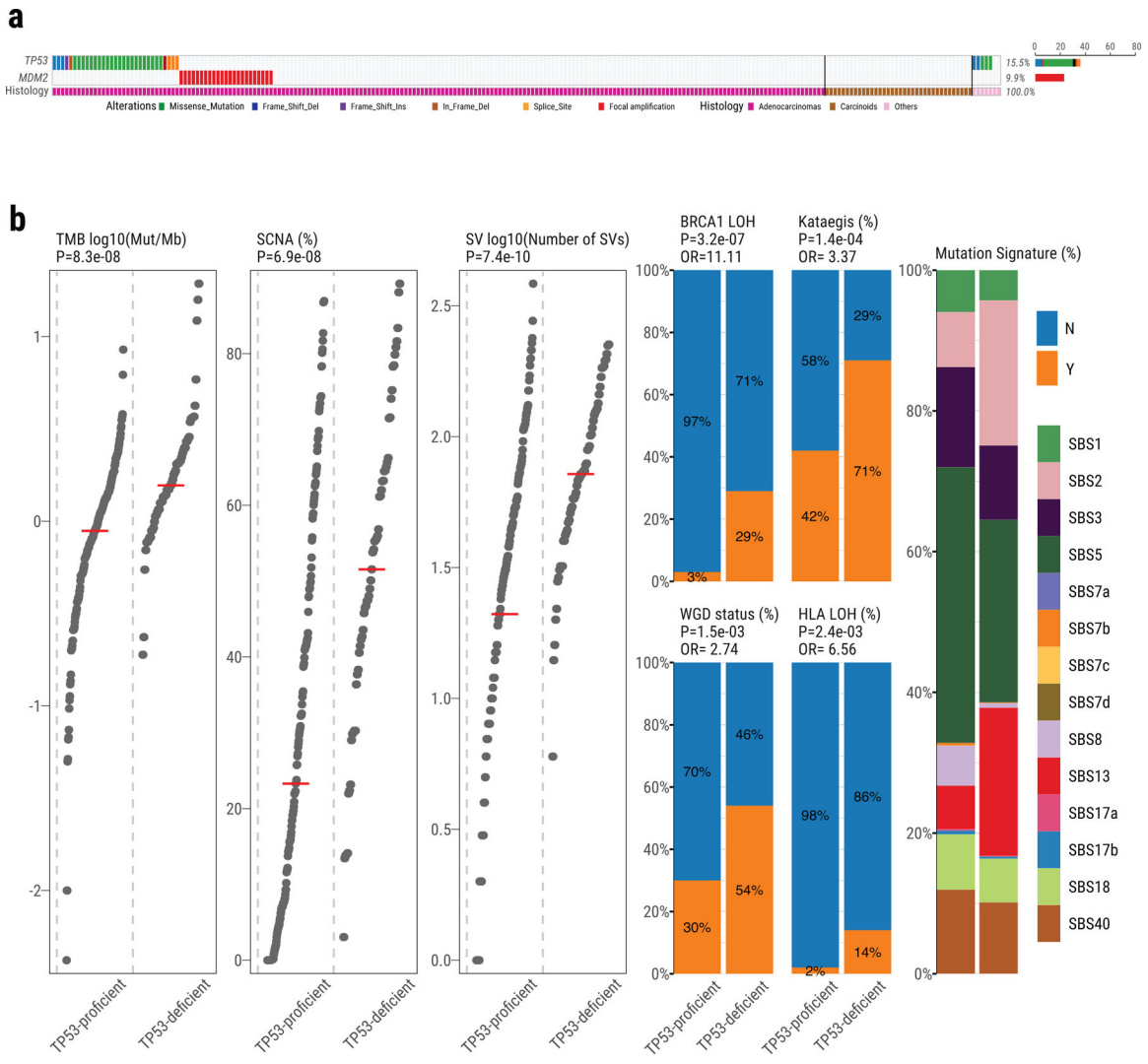

Extended Data Fig. 2. Genomic alterations of *TP53* pathway in Sherlock-*Lung*.

a, Oncoplot showing the mutual exclusivity between *TP53* mutations and *MDM2* amplification, which was used to define the TP53 proficient and deficient groups. The bottom bar shows tumor histological types. **b**, Comparison of genomic features between TP53-proficient and TP53-deficient tumors. Left three panels: tumor mutation burden, percentage of genome with SCNA and SV burden. *P*-values are calculated using the two-sided Mann-Whitney U test. Middle four panels: enrichments for *BRCA1* LOH, Kataegis events, WGD events, and HLA LOH. P-values and OR are calculated using Fisher's exact test (two-sided). Right panel: Contributions of each SBS signature.

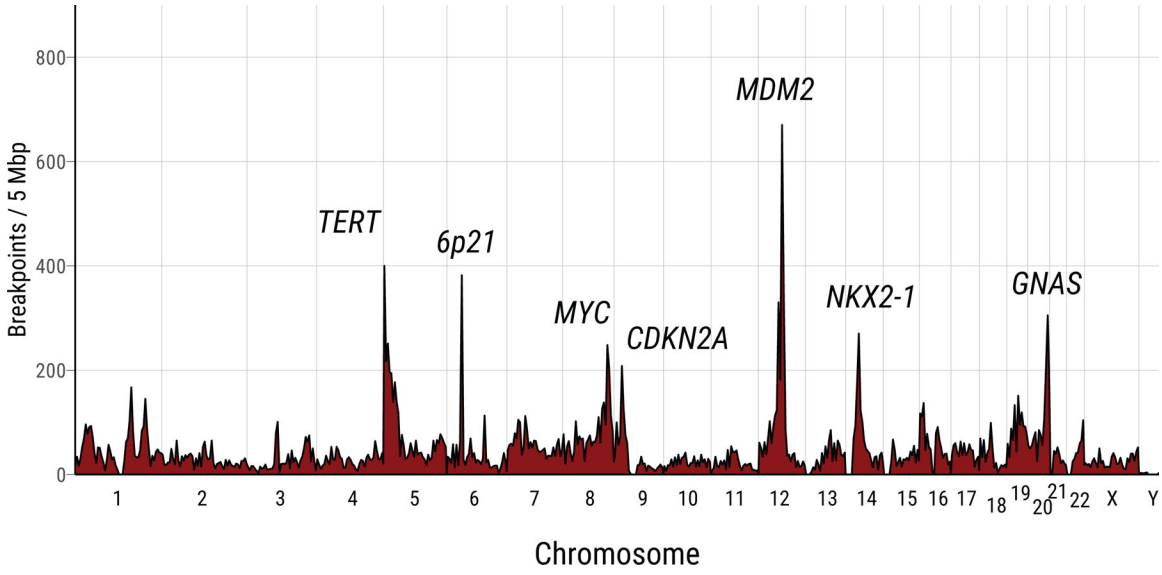

Extended Data Fig. 3. Recurrence of SV breakpoints in Sherlock-*Lung*.

The frequencies of chromosomal breakpoints are calculated using 5 Mb as a window across the whole genome.

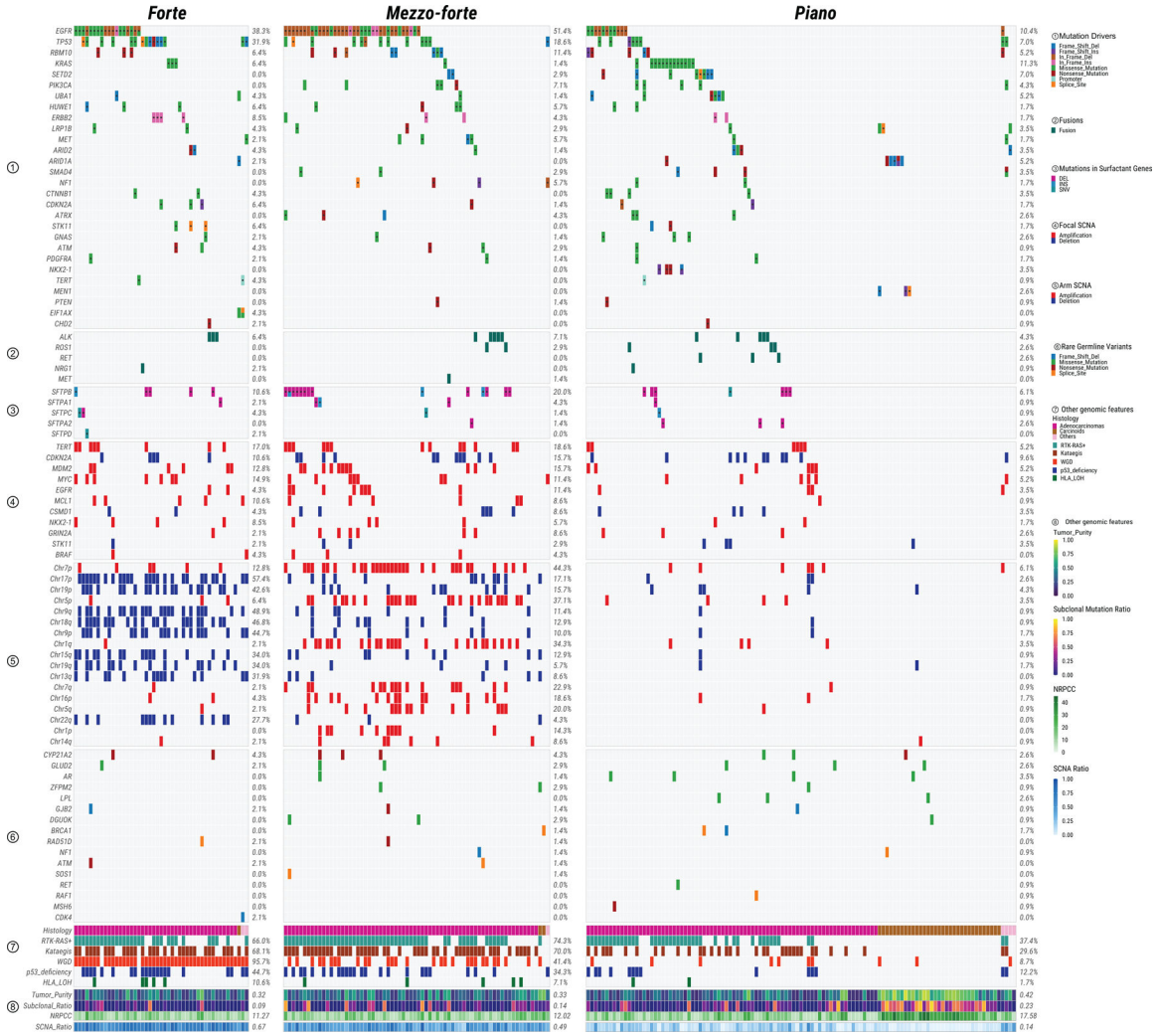

Extended Data Fig. 4. Summary of genomic features in LCINS based on different SCNA clusters.

Panels from top to bottom describe: 1) most frequently mutated or potential driver genes; 2) oncogenic fusions; 3) somatic mutations in surfactant associated genes; 4) significant focal SCNAs; 5) significant arm-level SCNAs; 6) genes with rare germline mutations; 7) and 8) other genomic features. The numbers on the right panel show the overall frequency (1–7) or median values (8). NRPCC: the number of reads per clonal copy.

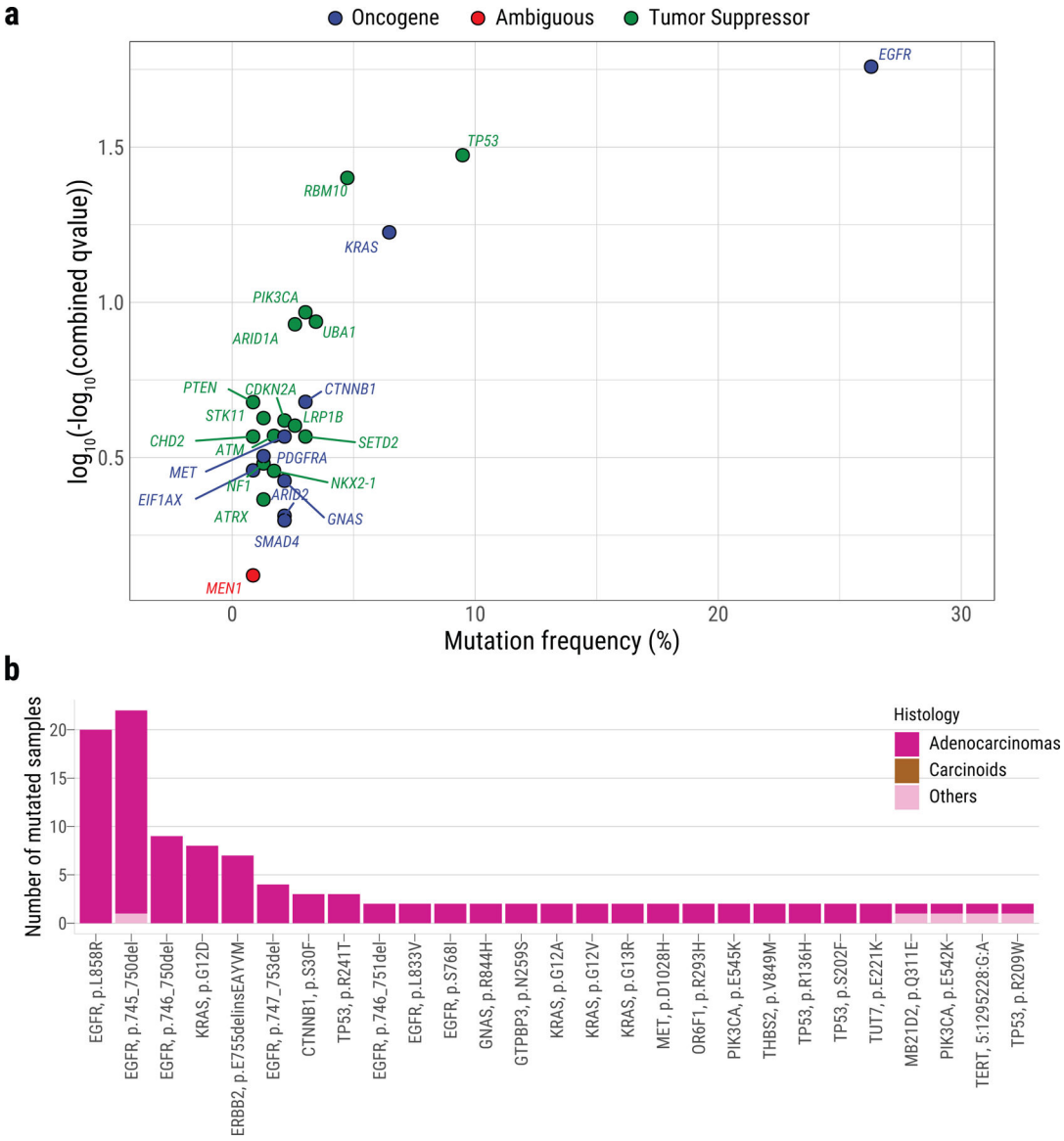

Extended Data Fig. 5. Genes with signals of positive selection in Sherlock-*Lung*.

a, The scatter plot showing significantly mutated genes according to IntOGen *q*-value <0.05 (y-axis) and mutational frequency in the cohort (x-axis). Genes are colored according to their inferred mode of action in tumorigenesis. **b**, Recurrent non-synonymous driver mutations (in ≥2 patients).

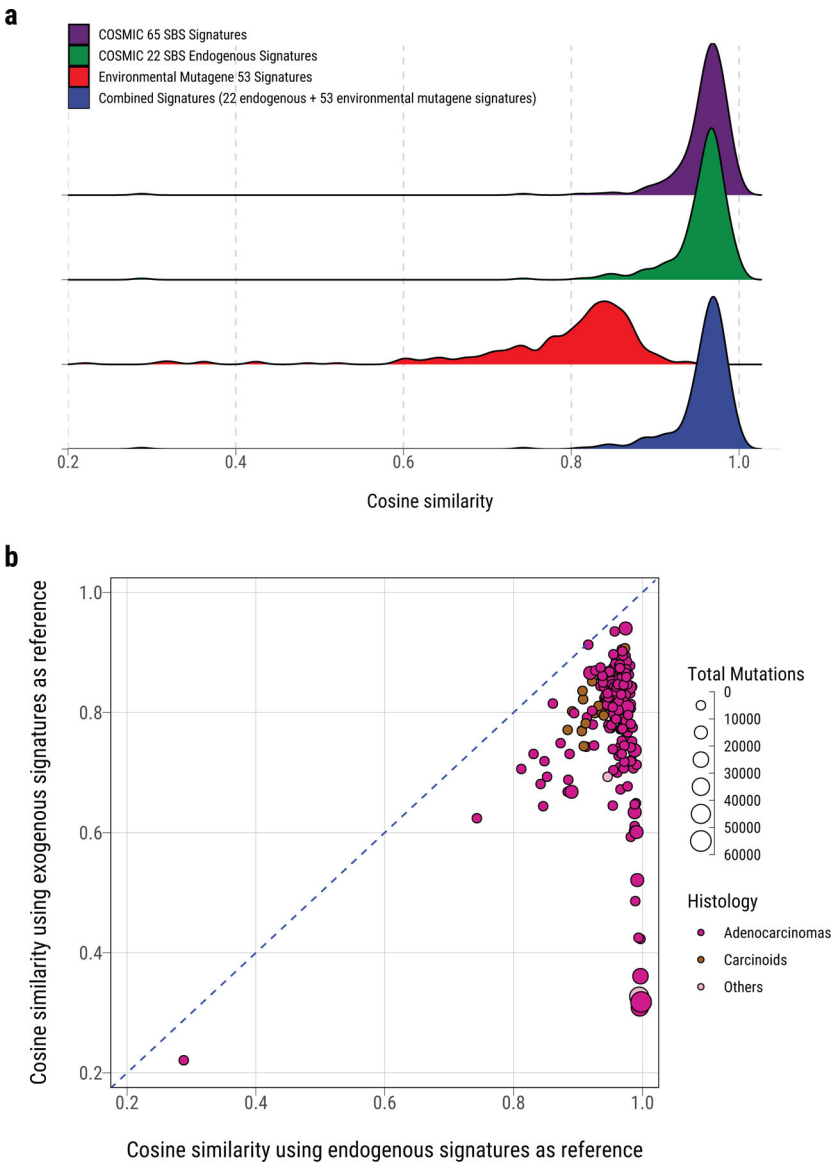

Extended Data Fig. 6. Dominant endogenous processes in Sherlock-*Lung*.

a, Density plot of cosine similarity between original mutational profile and reconstructed mutational profile using reference signatures from (top to bottom): 65 COSMIC SBS signatures, 22 COSMIC SBS signatures for endogenous processes, 53 MutaGene SBS signatures of environmental exposures, and a combined set of signatures including the 22 endogenous and 53 environmental exposure signatures. **b**, Comparison of the cosine similarity between the original mutational profiles and reconstructed mutational profiles using endogenous and exogenous signatures (similar to **a**). Each dot represents one sample. The size and color represent the total number of mutations and tumor histological type, respectively.

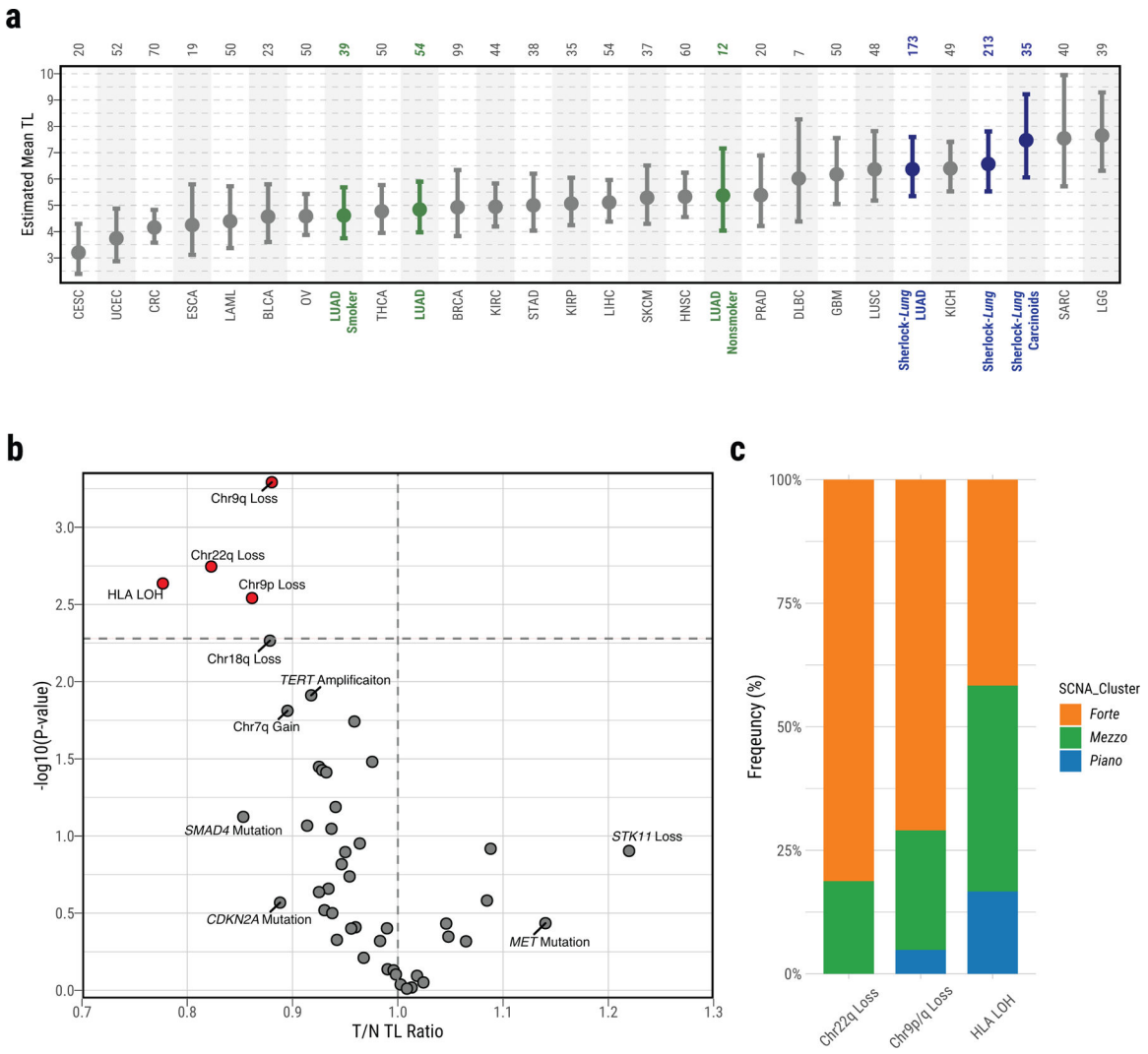

Extended Data Fig. 7. Association between T/N TL ratio and somatic alterations in Sherlock-*Lung*.

a, Distribution of mean telomere lengths (TL) in Sherlock-*Lung* (dark blue, overall and by histological type), TCGA LUAD (green, overall and by smoking status) and TCGA other cancer types (Grey). Total sample numbers for each type are shown at the top. Error bars, 95% CIs from linear mixed model. **b**, Scatterplot showing association between T/N TL ratio and somatic alterations. Association *P*-values (two-sided t-test; *FDR* adjusted using Benjamini-Hochberg method) are shown on the y-axis. Genomic alterations with *FDR* <=0.1 or T/N TL ratio >1.1 or <0.9 are labeled and further highlighted in red when significant (*FDR*=0.05; horizontal dashed line). **c**, The proportion of each SCNA cluster among the group of tumors with somatic alterations significantly associated with shorten T/N TL including Chr22q Loss, Chr9p/q Loss or HLA LOH.

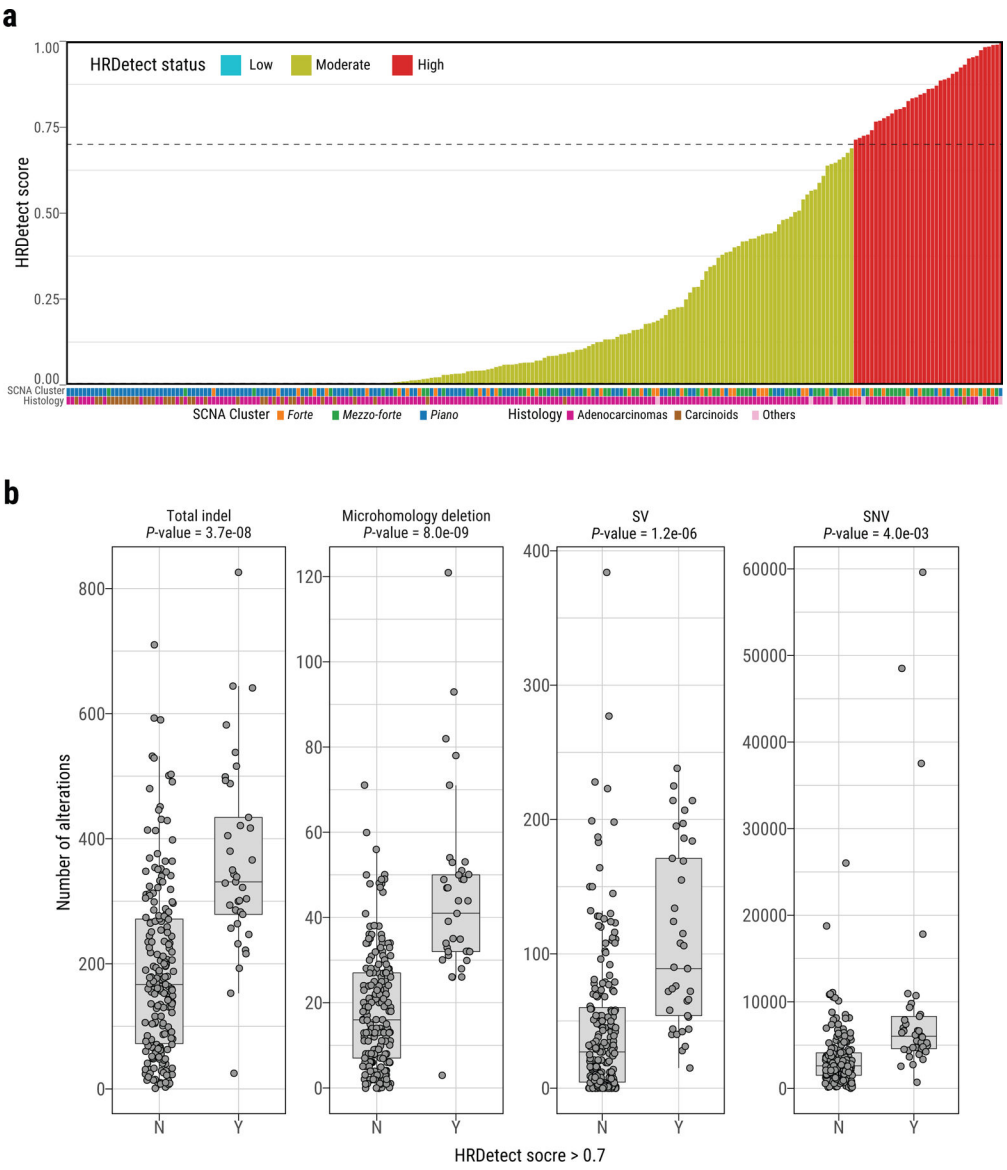

Extended Data Fig. 8. Homologous recombination deficiency (HRD) in Sherlock-*Lung*.

a, HRDetect scores of Sherlock-Lung samples. HRD-high: >0.7, HRD-low: < 0.005. **b**, Comparison of the number of total indels, microhomology deletions, SVs, and SNVs between samples with HRDetect score below 0.7 (group N) and above 0.7 (group Y). *P*-values are calculated using the two-sided Mann-Whitney U test. For box plots, center lines show the medians; box limits indicate the 25th and 75th percentiles; whiskers extend 1.5 times the interquartile range from the 25th and 75th percentiles.

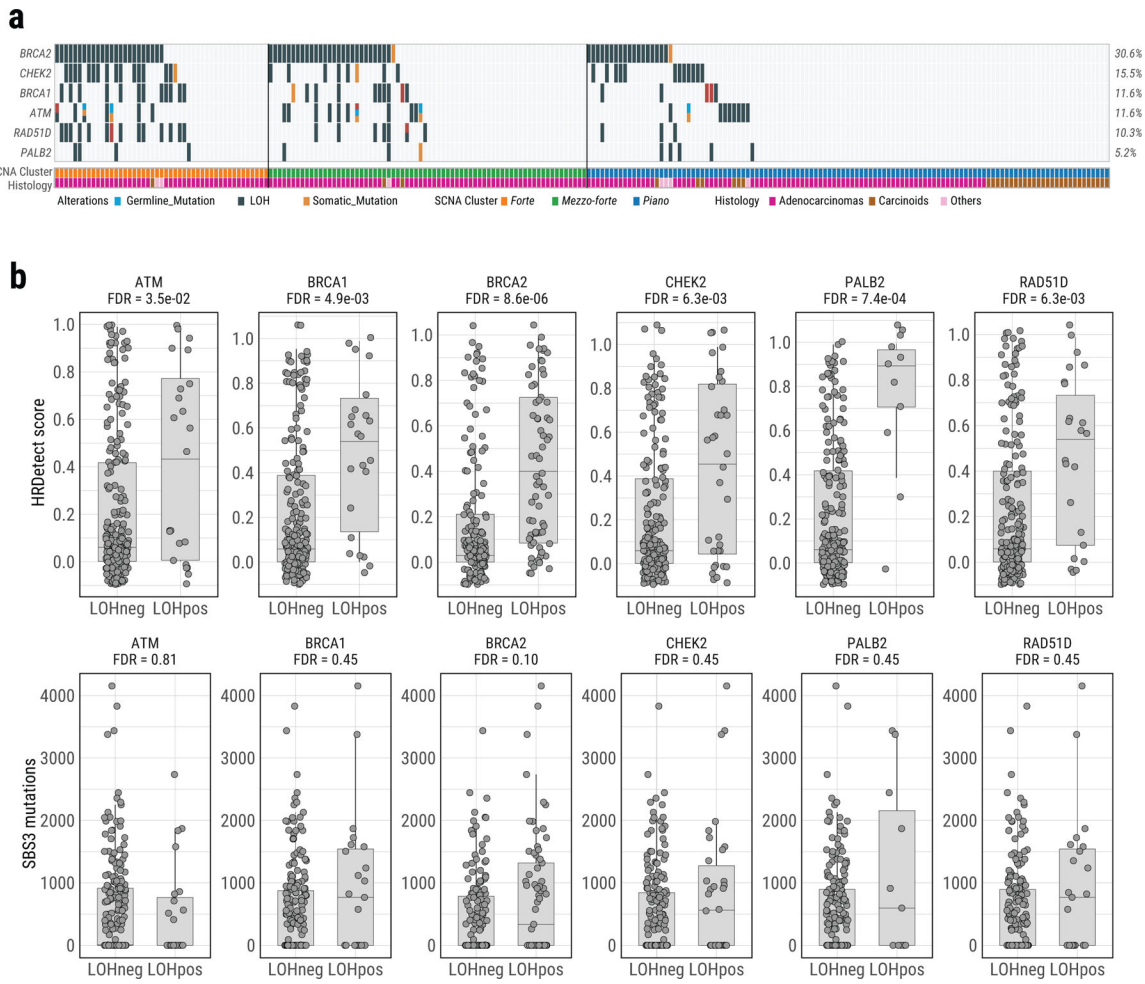

Extended Data Fig. 9. Genomic alterations in HRD associated genes in Sherlock-*Lung*.

a, Oncoplot of genomic alterations in HRD associated genes, including germline mutations, somatic mutations and LOH. Samples with biallelic alterations are represented by bars with two different colors. The bottom bar shows tumor histological types. **b**, Boxplots of HRDetect scores (top) and SBS mutation loads (bottom) in tumors with and without LOH of six HR associated genes. *FDR* are calculated using the two-sided Mann-Whitney U test with multiple testing correction based on the Benjamini & Hochberg method. For box plots, center lines show the medians; box limits indicate the 25th and 75th percentiles; whiskers extend 1.5 times the interquartile range from the 25th and 75th percentiles.

Supplementary Material

Refer to Web version on PubMed Central for supplementary material.

Authors

Tongwu Zhang[1], Philippe Joubert[2], Naser Ansari-Pour[3], Wei Zhao[1], Phuc H. Hoang[1], Rachel Lokanga[4], Aaron L. Moye[5], Jennifer Rosenbaum[6], Abel Gonzalez-Perez[7], Francisco Martínez-Jiménez[7], Andrea Castro[8], Lucia Anna Muscarella[9],

Paul Hofman[10], Dario Consonni[11], Angela C. Pesatori[11,12], Michael Kebede[1], Mengying Li[1], Bonnie E. Gould Rothberg[13,14], Iliana Peneva[15,16], Matthew B. Schabath[17], Maria Luana Poeta[18], Manuela Costantini[19], Daniela Hirsch[4], Kerstin Heselmeyer-Haddad[4], Amy Hutchinson[1,20], Mary Olanich[1,20], Scott M. Lawrence[1,20], Petra Lenz[1,20], Maire Duggan[21], Praphulla M.S. Bhawsar[1], Jian Sang[1], Jung Kim[1], Laura Mendoza[1], Natalie Saini[22], Leszek J. Klimczak[23], S. M. Ashiqul Islam[24], Burcak Otlu[24], Azhar Khandekar[24], Nathan Cole[1,20], Douglas R. Stewart[1], Jiyeon Choi[1], Kevin Brown[1], Neil E. Caporaso[1], Samuel H. Wilson[22], Yves Pommier[25], Qing Lan[1], Nathaniel Rothman[1], Jonas S. Almeida[1], Hannah Carter[8], Thomas Ried[4], Carla F Kim[5,26], Nuria Lopez-Bigas[7,27], Montserrat Garcia-Closas[1], Jianxin Shi[1], Yohan Bossé[2,28], Bin Zhu[1], Dmitry A. Gordenin[22], Ludmil B. Alexandrov[24], Stephen J. Chanock[1], David C. Wedge[3,29], Maria Teresa Landi[1]

Affiliations

[1]Division of Cancer Epidemiology and Genetics, National Cancer Institute, Bethesda, MD, USA

[2]Institut universitaire de cardiologie et de pneumologie de Québec - Laval University, Quebec City, Canada

[3]Big Data Institute, Nuffield Department of Medicine, University of Oxford, Oxford, UK

[4]Cancer Genomics Section, Center for Cancer Research, National Cancer Institute, Bethesda, MD, USA

[5]Stem Cell Program and Divisions of Hematology/Oncology and Pulmonary Medicine, Boston Children's Hospital, Boston, MA, USA

[6]Westat, Rockville, MD, USA

[7]Institute for Research in Biomedicine (IRB Barcelona), The Barcelona Institute of Science and Technology, Barcelona, Spain

[8]Department of Medicine, Division of Medical Genetics, University of California San Diego, San Diego, CA, USA

[9]Laboratory of Oncology, Fondazione IRCCS Casa Sollievo della Sofferenza, San Giovanni Rotondo, Italy

[10]Laboratory of Clinical and Experimental Pathology, Biobank 0033-00025, FHU OncoAge, Nice Hospital, University Côte d'Azur, Nice, France

[11]Fondazione IRCCS Ca' Granda, Ospedale Maggiore Policlinico, Milan, Italy

[12]Department of Clinical Sciences and Community Health, University of Milan, Milan, Italy

[13]Smilow Cancer Hospital, Yale-New Haven Health, New Haven, CT, USA

[14]Yale Comprehensive Cancer Center, New Haven, CT, USA

[15]Wellcome Centre for Human Genetics, University of Oxford, Oxford, UK

[16]NIHR Oxford Biomedical Research Centre, Oxford University Hospitals NHS Foundation Trust, John Radcliffe Hospital, Oxford, UK

[17]Department of Cancer Epidemiology, H. Lee Moffitt Cancer Center & Research Institute, Tampa, FL, USA

[18]Department of Bioscience, Biotechnology and Biopharmaceutics, University of Bari, Bari, Italy

[19]Department of Urology, IRCCS Regina Elena National Cancer Institute, Rome, Italy

[20]Cancer Genomics Research Laboratory, Frederick National Laboratory for Cancer Research, Frederick, MD, USA

[21]Department of Pathology and Laboratory Medicine, Cumming School of Medicine, University of Calgary, Calgary, Alberta, Canada

[22]Genome Integrity and Structural Biology Laboratory, National Institute of Environmental Health Sciences, Research Triangle, NC, USA

[23]Integrative Bioinformatics Support Group, National Institute of Environmental Health Sciences, Research Triangle, NC, USA

[24]Department of Cellular and Molecular Medicine and Department of Bioengineering and Moores Cancer Center, University of California, San Diego, CA, USA

[25]Developmental Therapeutics Branch and Laboratory of Molecular Pharmacology, Center for Cancer Research, National Cancer Institute, Bethesda, MD, USA

[26]Department of Genetics, Harvard Medical School, Boston, MA, USA

[27]Institució Catalana de Recerca i Estudis Avançats (ICREA), Barcelona, Spain

[28]Department of Molecular Medicine, Laval University, Quebec City, Canada

[29]Manchester Cancer Research Centre, The University of Manchester, Manchester, UK

Acknowledgments

This work has been supported by the Intramural Research Program (IRP) of the Division of Cancer Epidemiology and Genetics, National Cancer Institute, and the IRP of the National Institute of Environmental Health Sciences (Project number Z01 ES050159 to SHW, and Project number Z1AES103266 to DAG), US National Institutes of Health (NIH). This project was funded in whole or in part with Federal funds from the National Cancer Institute, National Institutes of Health, under Contract Nos. 75N91019D00024 and HHSN2612018000001I. The content of this publication does not necessarily reflect the views or policies of the US Department of Health and Human Services, nor does mention of trade names, commercial products, or organizations imply endorsement by the US government. The research was also supported by the Wellcome Trust Core Award, Grant Number 203141/Z/16/Z with funding from the NIHR Oxford BRC. L.B.A. is an Abeloff V scholar and he is personally supported by an Alfred P. Sloan Research Fellowship and a Packard Fellowship for Science and Engineering. Research at the L.B.A. Lab was also supported by NIEHS grant R01ES032547. The views expressed are those of the author(s) and not necessarily those of the NHS, the NIHR or the Department of Health. The collection of samples from the Institut universitaire de cardiologie et de pneumologie de Québec – Université Laval (IUCPQ-UL) was supported by the IUCPQ Foundation. GR Program 2010–2316264 supported L.A.M for samples collection by IRCCS Fondazione Casa Sollievo della Sofferenza. A.L.M. is supported by a Damon Runyon Cancer Research Foundation postdoctoral fellowship (DRG:2368–19) and a Postdoctoral Enrichment Program Award from the Burroughs Wellcome Fund

(1019903). C.F.K is supported in part by R35HL150876–01, the Thoracic Foundation, the Ellison Foundation, American Lung Association LCD-619492, and the Harvard Stem Cell Institute. N.L-B. acknowledges funding from the European Research Council (consolidator grant 682398). P.H. is supported in part by the "Association pour la Recherche contre le Cancer" (ARC CANC'AIR GENExposomics project). This work has been supported in part by the Tissue Core at the H. Lee Moffitt Cancer Center & Research Institute, a comprehensive cancer center designated by the National Cancer Institute and funded in part by Moffitt's Cancer Center Support Grant (P30-CA076292). B.E.G.R is supported by NIH 1P50 CA196530–01 and NIH 1K08 CA151645–01.

We thank the Sherlock-*Lung* study Scientific Advisory Board (Drs. Matthew Meyerson, Jonathan Samet, Margaret Spitz, Ronald Summers, Michael Thun, and Bill Travis) for their support. We also thank Dr. Yulia Rubanova from Toronto University for her help with the TrackSig analysis. The authors also would like to thank the staff at the IUCPQ-UL Biobank, Nice Biobank CRB, Yale University and Moffitt Cancer Center & Research Institute for their valuable assistance in collecting samples and corresponding clinical data. This work utilized the computational resources of the NIH high-performance computational capabilities Biowulf cluster (http://hpc.nih.gov).

References

1. The Cancer Atlas: Lung Cancer. The Cancer Atlashttps://canceratlas.cancer.org/the-burden/lung-cancer/.
2. Cho J. et al.Proportion and clinical features of never-smokers with non-small cell lung cancer. Chin. J. Cancer36, 20 (2017). [PubMed: 28179026]
3. Campbell JDet al.Distinct patterns of somatic genome alterations in lung adenocarcinomas and squamous cell carcinomas. Nat. Genet48, 607–616 (2016). [PubMed: 27158780]
4. Cancer Genome Atlas Research Network. Comprehensive molecular profiling of lung adenocarcinoma. Nature511, 543–550 (2014). [PubMed: 25079552]
5. Chen J. et al.Genomic landscape of lung adenocarcinoma in East Asians. Nat. Genet52, 177–186 (2020). [PubMed: 32015526]
6. Govindan R. et al.Genomic landscape of non-small cell lung cancer in smokers and never-smokers. Cell150, 1121–1134 (2012). [PubMed: 22980976]
7. Imielinski M. et al.Mapping the hallmarks of lung adenocarcinoma with massively parallel sequencing. Cell150, 1107–1120 (2012). [PubMed: 22980975]
8. Lee JJ-Ket al.Tracing Oncogene Rearrangements in the Mutational History of Lung Adenocarcinoma. Cell177, 1842–1857.e21 (2019). [PubMed: 31155235]
9. Shi J. et al.Somatic Genomics and Clinical Features of Lung Adenocarcinoma: A Retrospective Study. PLoS Med13, e1002162 (2016). [PubMed: 27923066]
10. Wang C. et al.Whole-genome sequencing reveals genomic signatures associated with the inflammatory microenvironments in Chinese NSCLC patients. Nat. Commun9, 2054 (2018). [PubMed: 29799009]
11. Fernandez-Cuesta L. et al.Frequent mutations in chromatin-remodelling genes in pulmonary carcinoids. Nat. Commun5, 3518 (2014). [PubMed: 24670920]
12. PCAWG. Pan-cancer analysis of whole genomes. Nature578, 82–93 (2020). [PubMed: 32025007]
13. Wu K. et al.Frequent alterations in cytoskeleton remodelling genes in primary and metastatic lung adenocarcinomas. Nat. Commun6, 10131 (2015). [PubMed: 26647728]
14. Carrot-Zhang J. et al.Whole-genome characterization of lung adenocarcinomas lacking the RTK/RAS/RAF pathway. Cell Rep34, 108707 (2021). [PubMed: 33535033]
15. Landi MTet al.Tracing Lung Cancer Risk Factors through Mutational Signatures in Never Smokers: the Sherlock-Lung Study. American Journal of Epidemiology (2020).
16. Skoulidis F. et al.Co-occurring genomic alterations define major subsets of KRAS-mutant lung adenocarcinoma with distinct biology, immune profiles, and therapeutic vulnerabilities. Cancer Discov5, 860–877 (2015). [PubMed: 26069186]
17. Moll UM & Petrenko O The MDM2-p53 interaction. Mol. Cancer Res 1, 1001–1008 (2003). [PubMed: 14707283]
18. Wala JAet al.Selective and mechanistic sources of recurrent rearrangements across the cancer genome. bioRxiv187609 (2017) doi:10.1101/187609.
19. Reznik E. et al.Mitochondrial DNA copy number variation across human cancers. Elife5, (2016).

20. McGranahan N. et al.Allele-Specific HLA Loss and Immune Escape in Lung Cancer Evolution. Cell171, 1259–1271.e11 (2017). [PubMed: 29107330]
21. Bailey MHet al.Comprehensive Characterization of Cancer Driver Genes and Mutations. Cell173, 371–385.e18 (2018). [PubMed: 29625053]
22. Moudry P. et al.Ubiquitin-activating enzyme UBA1 is required for cellular response to DNA damage. Cell Cycle11, 1573–1582 (2012). [PubMed: 22456334]
23. Martínez-Jiménez F. et al.A compendium of mutational cancer driver genes. Nat. Rev. Cancer (2020) doi:10.1038/s41568-020-0290-x.
24. Huang K-Let al.Pathogenic Germline Variants in 10,389 Adult Cancers. Cell173, 355–370.e14 (2018). [PubMed: 29625052]
25. Staaf J. et al.Whole-genome sequencing of triple-negative breast cancers in a population-based clinical study. Nat. Med25, 1526–1533 (2019). [PubMed: 31570822]
26. Alexandrov LBet al.The repertoire of mutational signatures in human cancer. Nature578, 94–101 (2020). [PubMed: 32025018]
27. Bergstrom ENet al.SigProfilerMatrixGenerator: a tool for visualizing and exploring patterns of small mutational events. BMC Genomics20, 685 (2019). [PubMed: 31470794]
28. Petljak M. et al.Characterizing Mutational Signatures in Human Cancer Cell Lines Reveals Episodic APOBEC Mutagenesis. Cell176, 1282–1294.e20 (2019). [PubMed: 30849372]
29. Jager M. et al.Deficiency of nucleotide excision repair is associated with mutational signature observed in cancer. Genome Res29, 1067–1077 (2019). [PubMed: 31221724]
30. Singh VK, Rastogi A, Hu X, Wang Y & De S Mutational signature SBS8 predominantly arises due to late replication errors in cancer. Commun Biol 3, 421 (2020). [PubMed: 32747711]
31. Roberts SAet al.An APOBEC cytidine deaminase mutagenesis pattern is widespread in human cancers. Nat. Genet45, 970–976 (2013). [PubMed: 23852170]
32. Kucab JEet al.A Compendium of Mutational Signatures of Environmental Agents. Cell177, 821–836.e16 (2019). [PubMed: 30982602]
33. Tokiwa H & Sera N Contribution of Nitrated Polycyclic Aromatic Hydrocarbons in Diesel Particles to Human Lung Cancer Induction. Polycycl. Aromat. Compd 21, 231–245 (2000).
34. Saini N. et al.Mutation signatures specific to DNA alkylating agents in yeast and cancers. Nucleic Acids Res48, 3692–3707 (2020). [PubMed: 32133535]
35. Chan K. et al.An APOBEC3A hypermutation signature is distinguishable from the signature of background mutagenesis by APOBEC3B in human cancers. Nat. Genet47, 1067–1072 (2015). [PubMed: 26258849]
36. Barthel FPet al.Systematic analysis of telomere length and somatic alterations in 31 cancer types. Nat. Genet49, 349–357 (2017). [PubMed: 28135248]
37. Feuerbach L. et al.TelomereHunter - in silico estimation of telomere content and composition from cancer genomes. BMC Bioinformatics20, 272 (2019). [PubMed: 31138115]
38. Davies H. et al.HRDetect is a predictor of BRCA1 and BRCA2 deficiency based on mutational signatures. Nat. Med23, 517–525 (2017). [PubMed: 28288110]
39. Zhao EYet al.Homologous Recombination Deficiency and Platinum-Based Therapy Outcomes in Advanced Breast Cancer. Clin. Cancer Res23, 7521–7530 (2017). [PubMed: 29246904]
40. Letouzé E. et al.Mutational signatures reveal the dynamic interplay of risk factors and cellular processes during liver tumorigenesis. Nat. Commun8, 1315 (2017). [PubMed: 29101368]
41. Shinde J. et al.Palimpsest: an R package for studying mutational and structural variant signatures along clonal evolution in cancer. Bioinformatics34, 3380–3381 (2018). [PubMed: 29771315]
42. Gerstung M. et al.The evolutionary history of 2,658 cancers. Nature578, 122–128 (2020). [PubMed: 32025013]
43. Halvorsen ARet al.TP53 Mutation Spectrum in Smokers and Never Smoking Lung Cancer Patients. Front. Genet7, 85 (2016). [PubMed: 27242894]
44. Gu J. et al.TP53 mutation is associated with a poor clinical outcome for non-small cell lung cancer: Evidence from a meta-analysis. Mol Clin Oncol5, 705–713 (2016). [PubMed: 28101350]
45. López S. et al.Interplay between whole-genome doubling and the accumulation of deleterious alterations in cancer evolution. Nat. Genet52, 283–293 (2020). [PubMed: 32139907]

46. Bielski CMet al.Genome doubling shapes the evolution and prognosis of advanced cancers. Nat. Genet50, 1189–1195 (2018). [PubMed: 30013179]
47. Jamal-Hanjani M. et al.Tracking the Evolution of Non-Small-Cell Lung Cancer. N. Engl. J. Med376, 2109–2121 (2017). [PubMed: 28445112]
48. International Agency for Research on Cancer. A Review of Human Carcinogens: Personal habits and indoor combustions (International Agency for Research on Cancer, 2012).
49. Office on Smoking and Health (US). The Health Consequences of Involuntary Exposure to Tobacco Smoke: A Report of the Surgeon General (Centers for Disease Control and Prevention (US), 2010).
50. Lopez-Bigas N & Gonzalez-Perez A Are carcinogens direct mutagens? Nature genetics vol. 52 1137–1138 (2020). [PubMed: 33128047]
51. Cho IJet al.Mechanisms, Hallmarks, and Implications of Stem Cell Quiescence. Stem Cell Reports12, 1190–1200 (2019). [PubMed: 31189093]
52. Fukada S-I, Ma Y & Uezumi A Adult stem cell and mesenchymal progenitor theories of aging. Front Cell Dev Biol 2, 10 (2014). [PubMed: 25364718]
53. Li L & Clevers H Coexistence of quiescent and active adult stem cells in mammals. Science 327, 542–545 (2010). [PubMed: 20110496]
54. Kim CFBet al.Identification of bronchioalveolar stem cells in normal lung and lung cancer. Cell121, 823–835 (2005). [PubMed: 15960971]
55. Van Meter MEMet al.K-RasG12D expression induces hyperproliferation and aberrant signaling in primary hematopoietic stem/progenitor cells. Blood109, 3945–3952 (2007). [PubMed: 17192389]
56. Kubara K. et al.Status of KRAS in iPSCs Impacts upon Self-Renewal and Differentiation Propensity. Stem Cell Reports11, 380–394 (2018). [PubMed: 29983389]
57. Bax M. et al.The Ubiquitin Proteasome System Is a Key Regulator of Pluripotent Stem Cell Survival and Motor Neuron Differentiation. Cells8, (2019).
58. Leon TYYet al.Transcriptional regulation of RET by Nkx2–1, Phox2b, Sox10, and Pax3. J. Pediatr. Surg44, 1904–1912 (2009). [PubMed: 19853745]
59. Grey W. et al.Activation of the receptor tyrosine kinase, RET, improves long-term hematopoietic stem cell outgrowth and potency. Blood (2020) doi:10.1182/blood.2020006302.
60. Fonseca-Pereira D. et al.The neurotrophic factor receptor RET drives haematopoietic stem cell survival and function. Nature514, 98–101 (2014). [PubMed: 25079320]
61. Zhao B. et al.ARID1A promotes genomic stability through protecting telomere cohesion. Nat. Commun10, 4067 (2019). [PubMed: 31492885]
62. Sun X. et al.Suppression of the SWI/SNF Component Arid1a Promotes Mammalian Regeneration. Cell Stem Cell18, 456–466 (2016). [PubMed: 27044474]
63. van der Vaart A & van den Heuvel S Switching on regeneration. Stem cell investigation vol. 3 41 (2016).
64. Wu S, Zhang R & Bitler BG Arid1a controls tissue regeneration. Stem cell investigation vol. 3 35 (2016). [PubMed: 27582418]
65. Nagl NG Jr, Wang X, Patsialou A, Van Scoy M & Moran E Distinct mammalian SWI/SNF chromatin remodeling complexes with opposing roles in cell-cycle control. EMBO J 26, 752–763 (2007). [PubMed: 17255939]
66. Chiba SNotch signaling in stem cell systems. Stem Cells24, 2437–2447 (2006). [PubMed: 16888285]
67. Yoshida K. et al.Tobacco smoking and somatic mutations in human bronchial epithelium. Nature (2020) doi:10.1038/s41586-020-1961-1.
68. Maeda Y, Davé V & Whitsett JA Transcriptional control of lung morphogenesis. Physiol. Rev 87, 219–244 (2007). [PubMed: 17237346]
69. Alanis DM, Chang DR, Akiyama H, Krasnow MA & Chen J Two nested developmental waves demarcate a compartment boundary in the mouse lung. Nat. Commun 5, 3923 (2014). [PubMed: 24879355]
70. Singh I. et al.Hmga2 is required for canonical WNT signaling during lung development. BMC Biol12, 21 (2014). [PubMed: 24661562]

71. Laughney AMet al.Regenerative lineages and immune-mediated pruning in lung cancer metastasis. Nat. Med26, 259–269 (2020). [PubMed: 32042191]

72. Duffy MJet al.p53 as a target for the treatment of cancer. Cancer Treat. Rev40, 1153–1160 (2014). [PubMed: 25455730]

73. Shaikh MFet al.Emerging Role of MDM2 as Target for Anti-Cancer Therapy: A Review. Ann. Clin. Lab. Sci46, 627–634 (2016). [PubMed: 27993876]

74. Chuang JCet al.ERBB2-Mutated Metastatic Non-Small Cell Lung Cancer: Response and Resistance to Targeted Therapies. J. Thorac. Oncol12, 833–842 (2017). [PubMed: 28167203]

75. Harvey RD, Adams VR, Beardslee T & Medina P Afatinib for the treatment of EGFR mutation-positive NSCLC: A review of clinical findings. J. Oncol. Pharm. Pract 1078155220931926 (2020).

76. Park K. et al.Afatinib versus gefitinib as first-line treatment of patients with EGFR mutation-positive non-small-cell lung cancer (LUX-Lung 7): a phase 2B, open-label, randomised controlled trial. Lancet Oncol17, 577–589 (2016). [PubMed: 27083334]

77. Shen X. et al.A systematic analysis of the resistance and sensitivity of HER2YVMA receptor tyrosine kinase mutant to tyrosine kinase inhibitors in HER2-positive lung cancer. J. Recept. Signal Transduct. Res36, 89–97 (2016). [PubMed: 26391018]

78. Miyazaki M. et al.The p53 activator overcomes resistance to ALK inhibitors by regulating p53-target selectivity in ALK-driven neuroblastomas. Cell Death Discov4, 56 (2018). [PubMed: 29760954]

79. Dey P. et al.Genomic deletion of malic enzyme 2 confers collateral lethality in pancreatic cancer. Nature542, 119–123 (2017). [PubMed: 28099419]

80. Muller FL, Aquilanti EA & DePinho RA Collateral Lethality: A new therapeutic strategy in oncology. Trends Cancer Res 1, 161–173 (2015).

81. Hsiehchen D. et al.DNA Repair Gene Mutations as Predictors of Immune Checkpoint Inhibitor Response beyond Tumor Mutation Burden. Cell Rep Med1, (2020).

82. Rizvi NAet al.Cancer immunology. Mutational landscape determines sensitivity to PD-1 blockade in non-small cell lung cancer. Science348, 124–128 (2015). [PubMed: 25765070]

83. Hellmann MDet al.Nivolumab plus Ipilimumab in Lung Cancer with a High Tumor Mutational Burden. N. Engl. J. Med378, 2093–2104 (2018). [PubMed: 29658845]

84. Ready N. et al.First-Line Nivolumab Plus Ipilimumab in Advanced Non-Small-Cell Lung Cancer (CheckMate 568): Outcomes by Programmed Death Ligand 1 and Tumor Mutational Burden as Biomarkers. J. Clin. Oncol37, 992–1000 (2019). [PubMed: 30785829]

85. Canon J. et al.The clinical KRAS(G12C) inhibitor AMG 510 drives anti-tumour immunity. Nature575, 217–223 (2019). [PubMed: 31666701]

86. Yang L. et al.Targeting cancer stem cell pathways for cancer therapy. Signal Transduct Target Ther5, 8 (2020). [PubMed: 32296030]

87. Medema JP & Vermeulen L Microenvironmental regulation of stem cells in intestinal homeostasis and cancer. Nature 474, 318–326 (2011). [PubMed: 21677748]

Method References

88. Jørsboe E, Hanghøj K & Albrechtsen A fastNGSadmix: admixture proportions and principal component analysis of a single NGS sample. Bioinformatics 33, 3148–3150 (2017). [PubMed: 28957500]

89. Cibulskis K. et al.Sensitive detection of somatic point mutations in impure and heterogeneous cancer samples. Nat. Biotechnol. 31, 213–219 (2013). [PubMed: 23396013]

90. Kim S. et al.Strelka2: fast and accurate calling of germline and somatic variants. Nat. Methods15, 591–594 (2018). [PubMed: 30013048]

91. Freed D, Pan R & Aldana R TNscope: Accurate Detection of Somatic Mutations with Haplotype-based Variant Candidate Detection and Machine Learning Filtering. bioRxiv 250647 (2018) doi:10.1101/250647.

92. Zhu B. et al.The genomic and epigenomic evolutionary history of papillary renal cell carcinomas. Nat. Commun11, 3096 (2020). [PubMed: 32555180]

93. Karczewski KJet al.Variation across 141,456 human exomes and genomes reveals the spectrum of loss-of-function intolerance across human protein-coding genes. bioRxiv531210 (2019) doi:10.1101/531210.
94. Ramos AHet al.Oncotator: cancer variant annotation tool. Hum. Mutat36, E2423–9 (2015). [PubMed: 25703262]
95. Wang K, Li M & Hakonarson H ANNOVAR: functional annotation of genetic variants from high-throughput sequencing data. Nucleic Acids Res 38, e164 (2010). [PubMed: 20601685]
96. Hasan MS, Wu X, Watson LT & Zhang L UPS-indel: a Universal Positioning System for Indels. Sci. Rep 7, 14106 (2017). [PubMed: 29074871]
97. Dentro SC, Wedge DC & Van Loo P Principles of Reconstructing the Subclonal Architecture of Cancers. Cold Spring Harb. Perspect. Med 7, (2017).
98. Nik-Zainal S. et al.The life history of 21 breast cancers. Cell149, 994–1007 (2012). [PubMed: 22608083]
99. Scott ADet al.CharGer: clinical Characterization of Germline variants. Bioinformatics35, 865–867 (2019). [PubMed: 30102335]
100. Landrum MJet al.ClinVar: public archive of interpretations of clinically relevant variants. Nucleic Acids Res44, D862–8 (2016). [PubMed: 26582918]
101. Martincorena I. et al.Universal Patterns of Selection in Cancer and Somatic Tissues. Cell171, 1029–1041.e21 (2017). [PubMed: 29056346]
102. Muiños F, Martinez-Jimenez F, Pich O, Gonzalez-Perez A & Lopez-Bigas N In silico saturation mutagenesis of cancer genes. bioRxiv 2020.06.03.130211 (2020) doi:10.1101/2020.06.03.130211.
103. Mermel CHet al.GISTIC2.0 facilitates sensitive and confident localization of the targets of focal somatic copy-number alteration in human cancers. Genome Biol12, R41 (2011). [PubMed: 21527027]
104. Dewhurst SMet al.Tolerance of whole-genome doubling propagates chromosomal instability and accelerates cancer genome evolution. Cancer Discov4, 175–185 (2014). [PubMed: 24436049]
105. Yang L. et al.Diverse mechanisms of somatic structural variations in human cancer genomes. Cell153, 919–929 (2013). [PubMed: 23663786]
106. Li Y. et al.Patterns of somatic structural variation in human cancer genomes. Nature578, 112–121 (2020). [PubMed: 32025012]
107. Ding Z. et al.Estimating telomere length from whole genome sequence data. Nucleic Acids Res42, e75 (2014). [PubMed: 24609383]
108. Alexandrov LBet al.Signatures of mutational processes in human cancer. Nature500, 415–421 (2013). [PubMed: 23945592]
109. Shukla SAet al.Comprehensive analysis of cancer-associated somatic mutations in class I HLA genes. Nat. Biotechnol33, 1152–1158 (2015). [PubMed: 26372948]
110. Bolli N. et al.Heterogeneity of genomic evolution and mutational profiles in multiple myeloma. Nat. Commun5, 2997 (2014). [PubMed: 24429703]
111. Luce RDIndividual choice behavior; a theoretical analysis. (Wiley, 1959).
112. Plackett RLThe Analysis of Permutations. Journal of the Royal Statistical Society. Series C (Applied Statistics)24, 193 (1975).

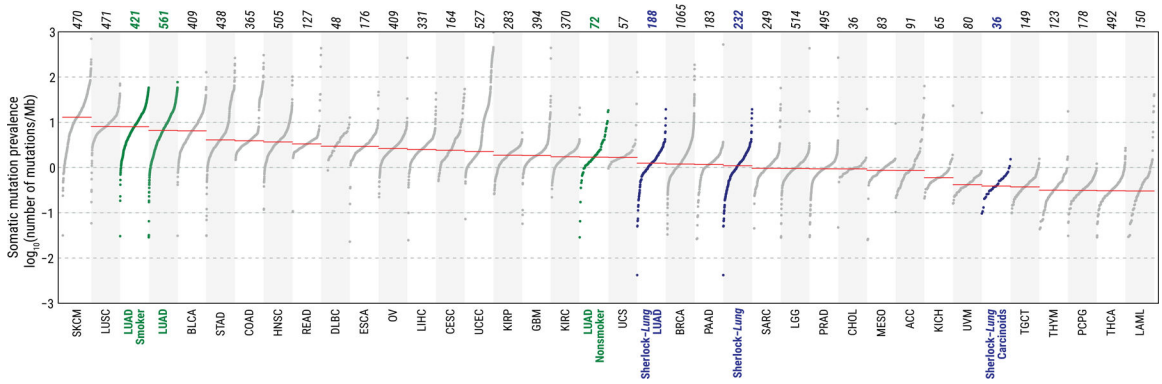

Fig. 1. Tumor mutational burden (TMB) across lung cancer in never smokers from the Sherlock-*Lung* study and 33 cancer types from the TCGA study.

The Sherlock-*Lung* samples (blue) are shown overall and by histological type. TCGA LUAD samples (green) are shown overall and by smoking status. Each dot represents a sample; total sample numbers for each type are shown at the top. The red horizontal lines are the median numbers of mutations per megabase ($\log_{10}$). On the bottom, acronyms of cancer types as in TCGA (https://gdc.cancer.gov/resources-tcga-users/tcga-code-tables/tcga-study-abbreviations).

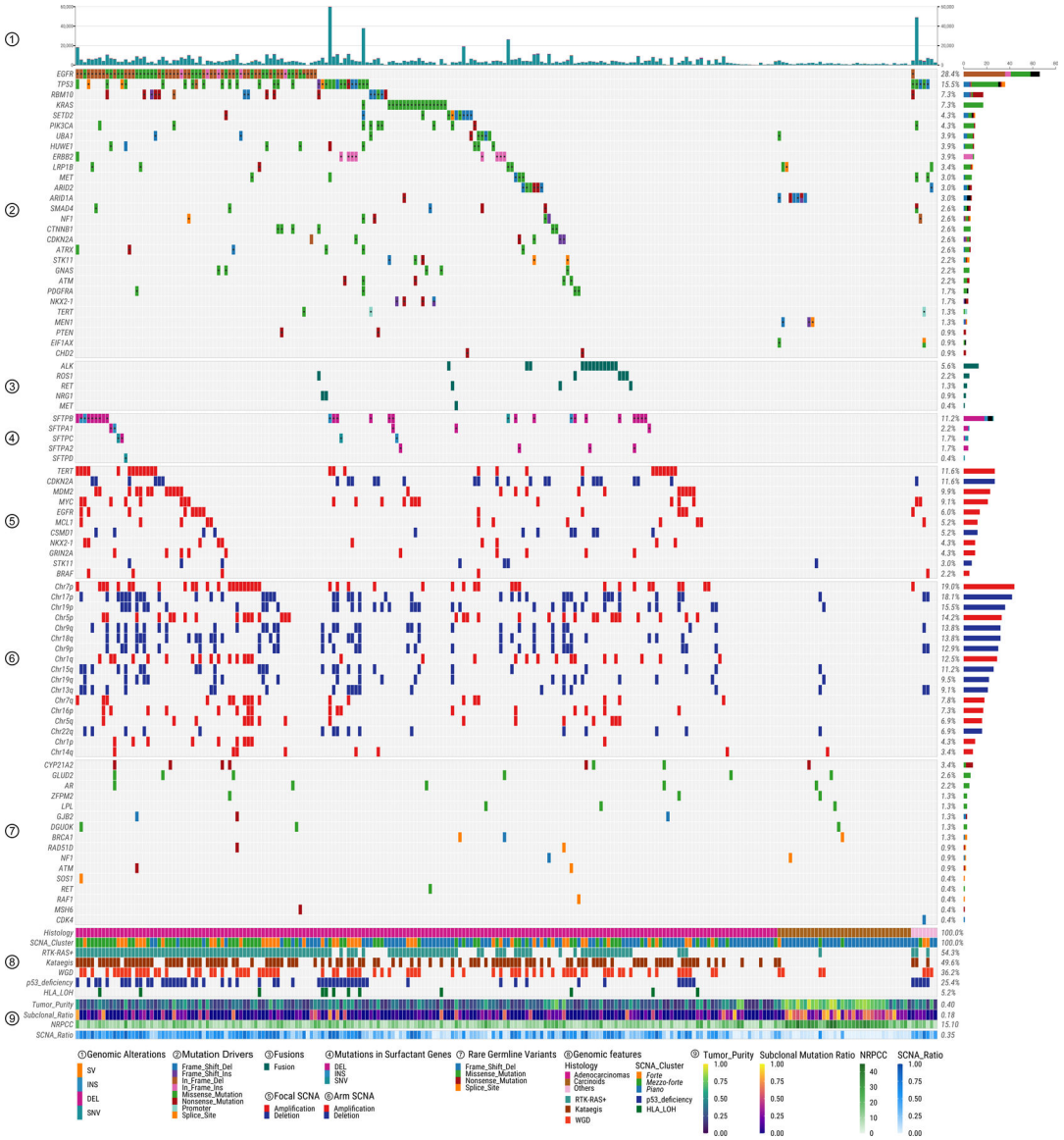

Fig. 2. Genomic characteristics of lung cancer in never smokers.

Panels from top to bottom describe: 1) distribution of genomic alteration numbers; 2) most frequently mutated or potential driver genes; 3) oncogenic fusions; 4) somatic mutations in surfactant associated genes; 5) significant focal SCNAs; 6) significant arm-level SCNAs; 7) genes with rare germline mutations; 8) and 9) different genomic features. The numbers on the right panel show the overall frequency (1–8) or median values (9). NRPCC: the number of reads per clonal copy.

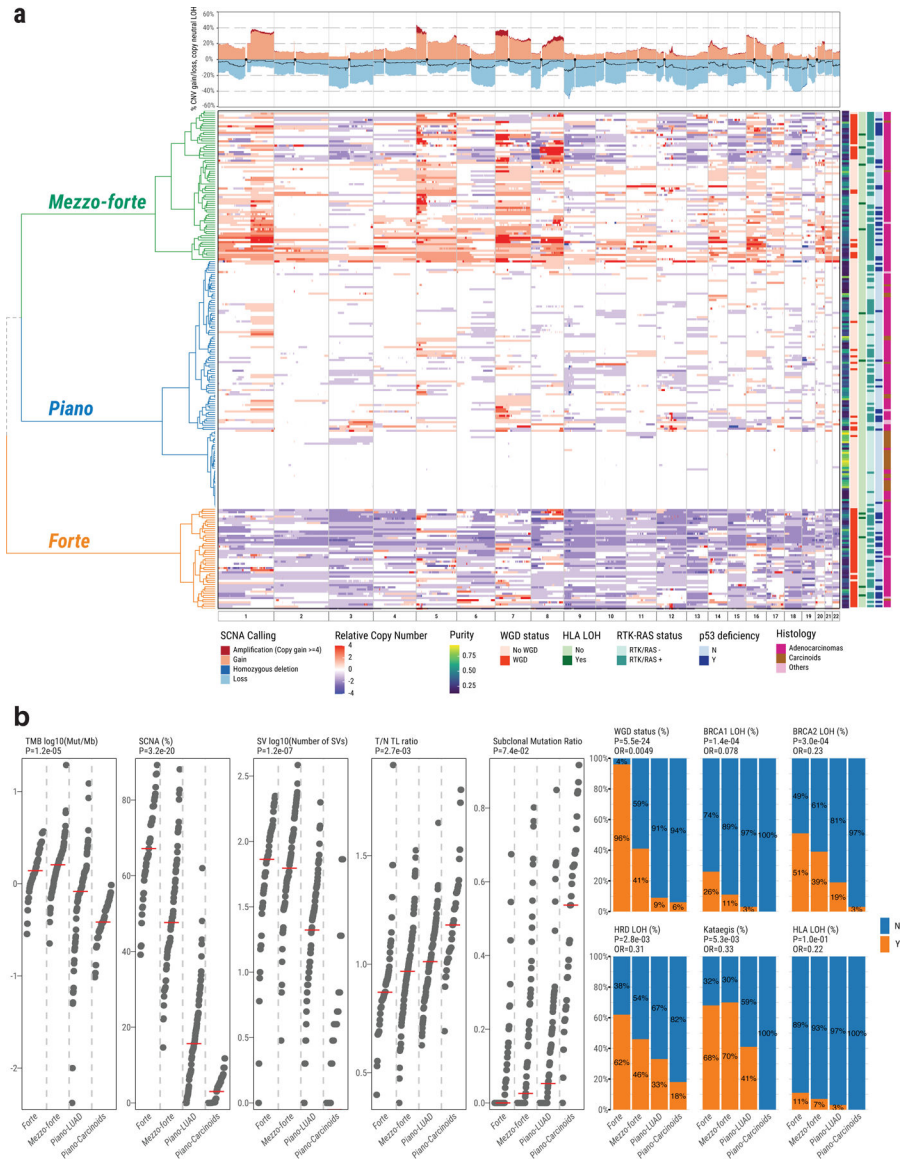

Fig. 3. Genomic classification of lung cancer in never smokers based on somatic copy number alterations.

a, Left panel shows unsupervised clustering of arm-level SCNA events: *piano*, *mezzo-forte* and *forte*. The relative copy number is calculated as: total copy number - ploidy (non-WGD=2 and WGD=4). Samples in rows are annotated by tumor purity, WGD status, HLA LOH, RTK-RAS status, TP53 deficiency, and tumor histological type. Top panel shows SCNA frequency including amplification, deletion and copy neutral LOH (black line). **b**, Comparison of genomic aberrations or features (Y="with", N="without") among *forte*, *mezzo-forte*, *piano*-LUAD, and *piano*-Carcinoids tumors. Left five panels: tumor mutation burden, percentage of genome with SCNAs, SV burden, T/N TL ratio and subclonal mutation ratio. *P*-values are calculated using two-sided Mann-Whitney U test. Right six panels: enrichments for WGD, Kataegis, *BRCA2* LOH, *BRCA1* LOH, HRD LOH and *HLA* LOH. *P*-values and *OR* are calculated using two-sided Fisher's exact test. All statistical analyses were performed between *forte* and *piano*-LUAD.

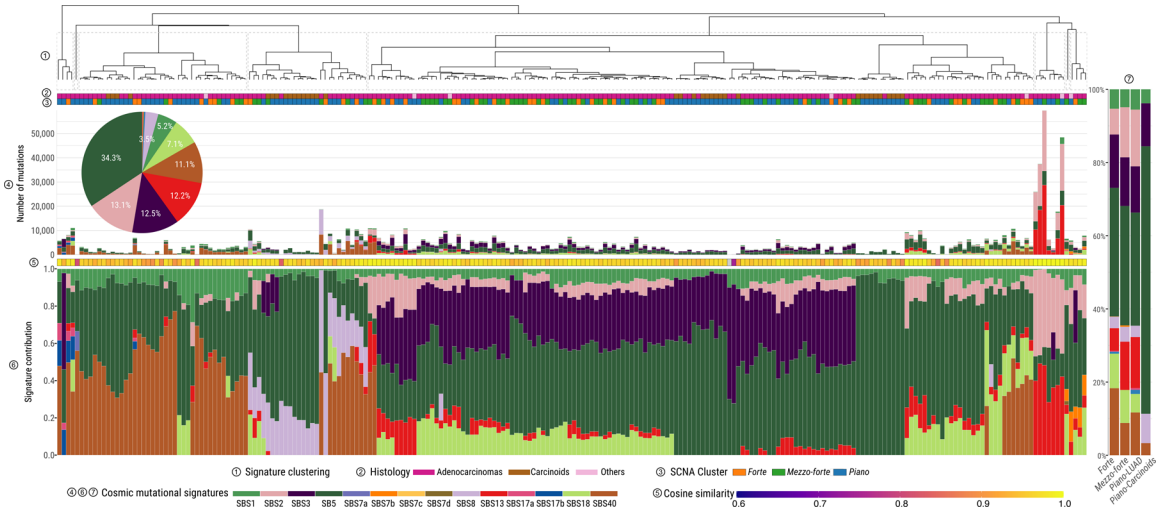

Fig. 4. Landscape of mutational processes in Sherlock-*Lung*.

Mutational signature profile of single base substitutions (SBS) across 232 Sherlock-*Lung* samples. Panels from top to bottom: 1) Unsupervised clustering based on the proportion of SBS signatures; 2) Tumor histological type; 3) SCNA cluster; 4) Pie chart showing the percentage of mutations contributed to each SBS signature and the barplot presenting the total number of SNVs assigned to each SBS signature; 5) Cosine similarity between original mutational profile and signature decomposition result; 6) Proportions of SBS mutational signatures in each sample. 7) Proportions of SBS mutational signatures in each SCNA subtype.

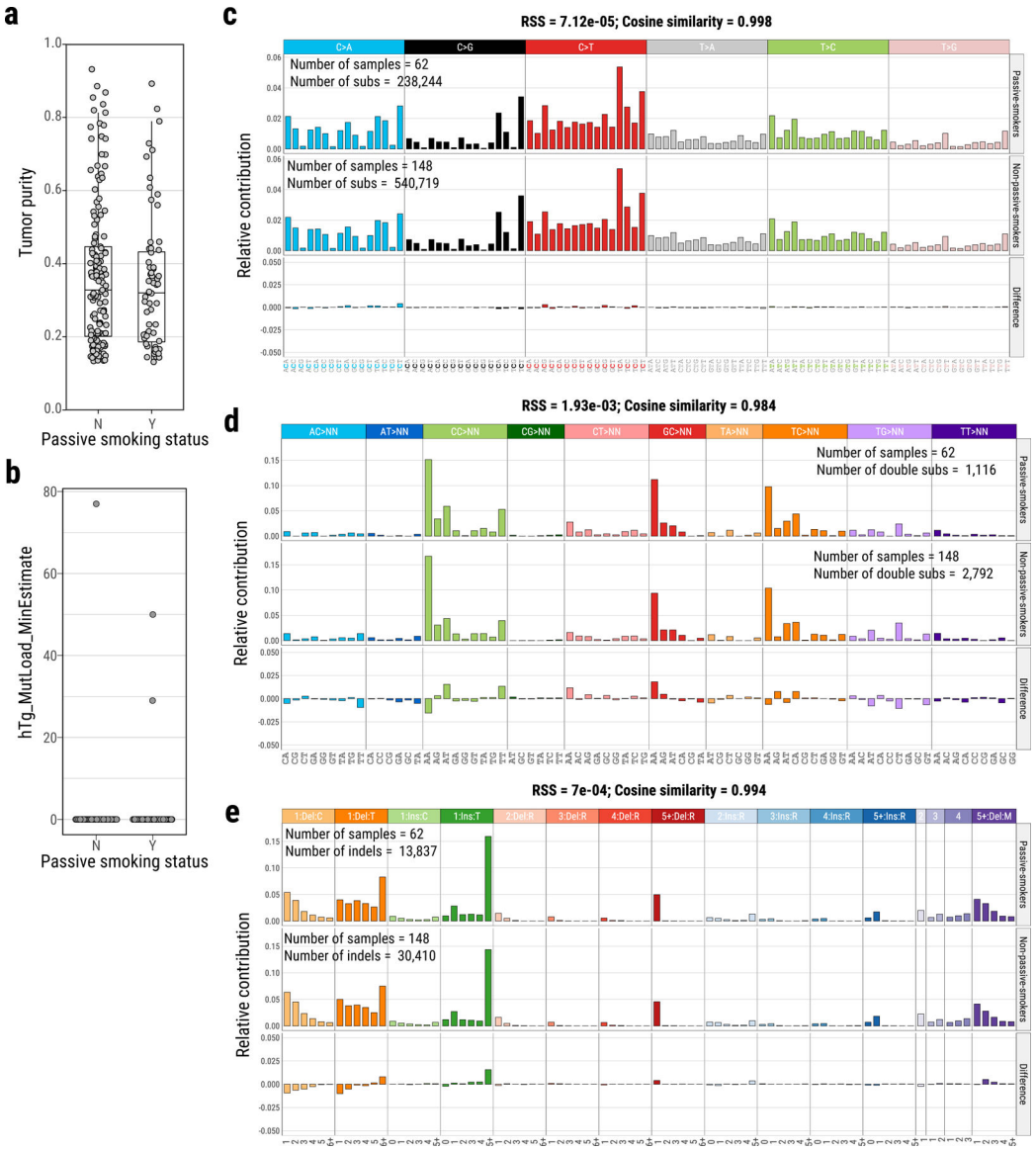

Fig. 5. Comparison of mutational spectra between passive smokers and non-passive smokers in Sherlock-*Lung*.

Identification of tumor purity **(a)** and alkylation-induced mutagenesis (hTg → hGg signature) **(b)** between passive smokers (Y, N=62) and non-passive smokers (N, N=148). Mutational spectra comparison of single base substitutions **(c)**, double base substitutions **(d)** and indels (e) between passive-smokers and non-passive smokers.

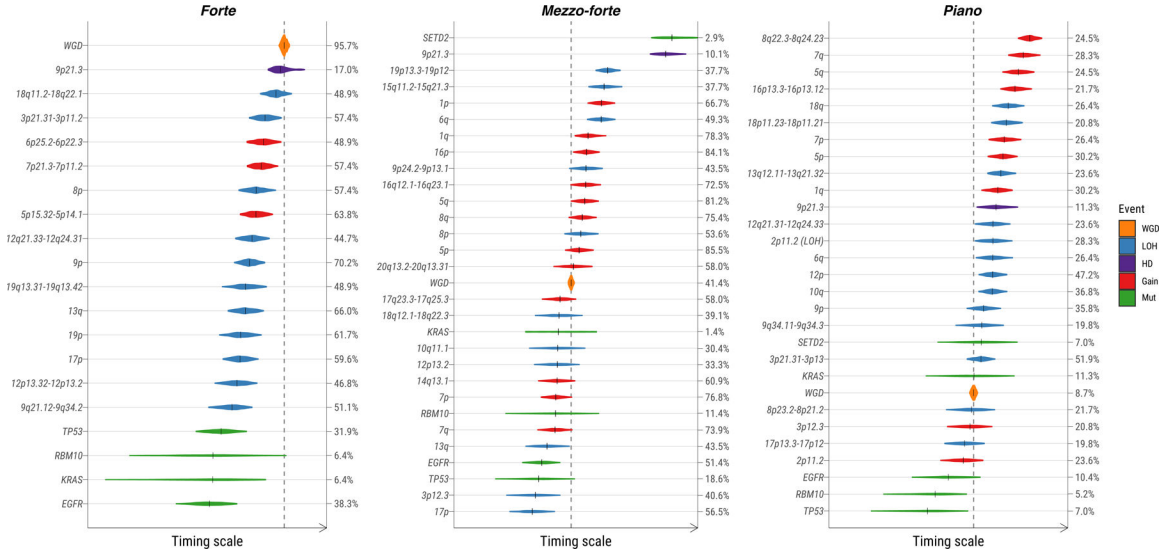

Fig. 6. Diagram of estimated ordering of significant SCNAs (including chromosome gains/losses and mutations) relative to WGD in three lung cancer subtypes based on SCNA clusters *forte*, *mezzo-forte* and *piano*.

The size of violin plots denotes the uncertainty of timing for specific events across all samples and the short black solid lines represent the median time. The vertical dashed line indicates the median time for WGD events. Ordering of genomic events was based on the PlacketLuce package model with 95% CI. The frequency of each event is labeled on the right y-axis.

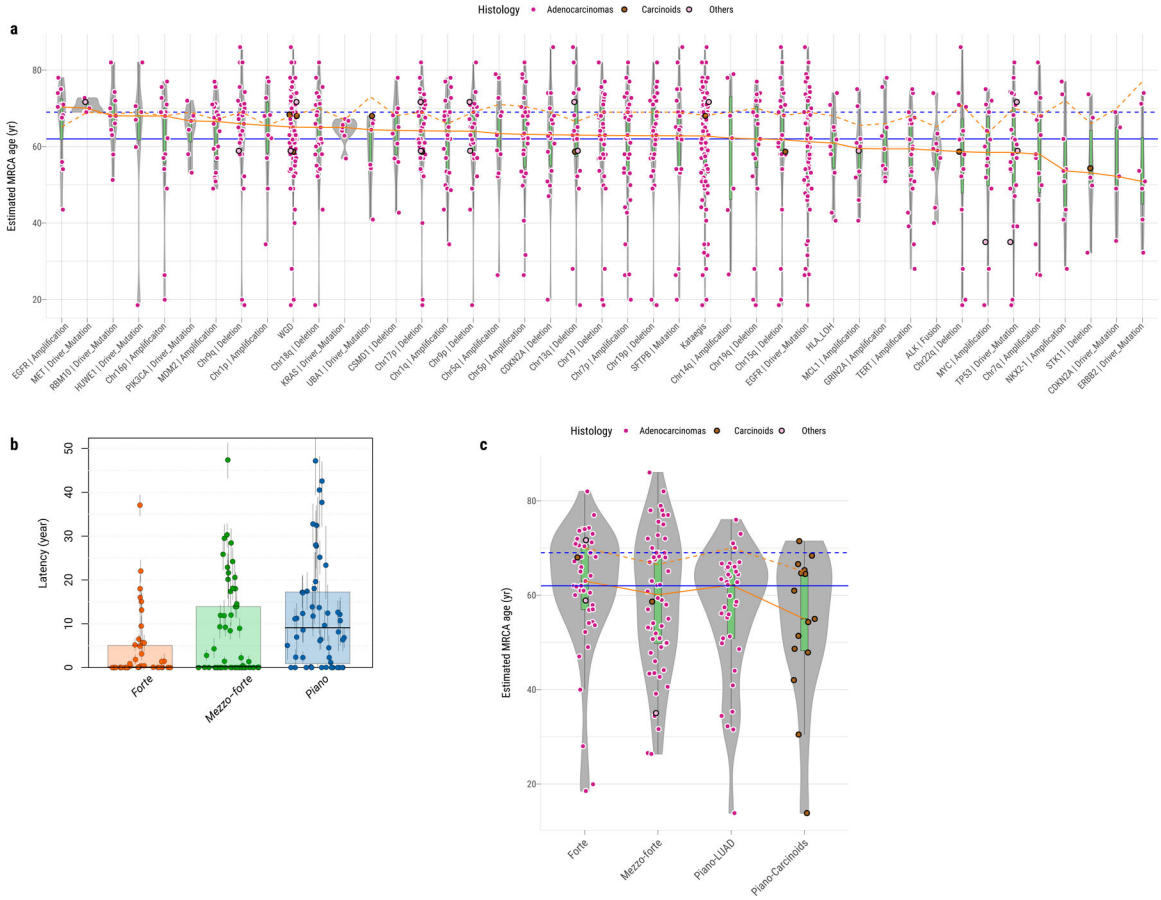

Fig. 7. Reconstruction of the evolutionary history of lung cancer in never smokers.

a, Estimated age at which the most recent common ancestor (MRCA) emerged in tumors (y-axis), grouped by genomic alterations or features (x-axis, frequency >3%) as shown in Figure 2. The color of each dot represents the tumor histological subtype. The orange solid and dashed lines indicate the median estimated MRCA age and the median age at diagnosis in the same group, respectively. The blue solid and dashed lines indicate the median estimated MRCA age and the median age at diagnosis in all samples, respectively. **b**, Boxplots show the latency between the MRCA and the age at diagnosis based on 1× acceleration rate across *forte*, *mezzo-forte*, and *piano* subtypes with 95% CI for each tumor. c, Similar to a, estimated MRCA age among SCNA subtypes: *forte*, *mezzo-forte*, *piano*-LUAD and *piano*-carcinoids. For box plots from a to c, center lines show the medians; box limits indicate the 25th and 75th percentiles; whiskers extend 1.5 times the interquartile range from the 25th and 75th percentiles.

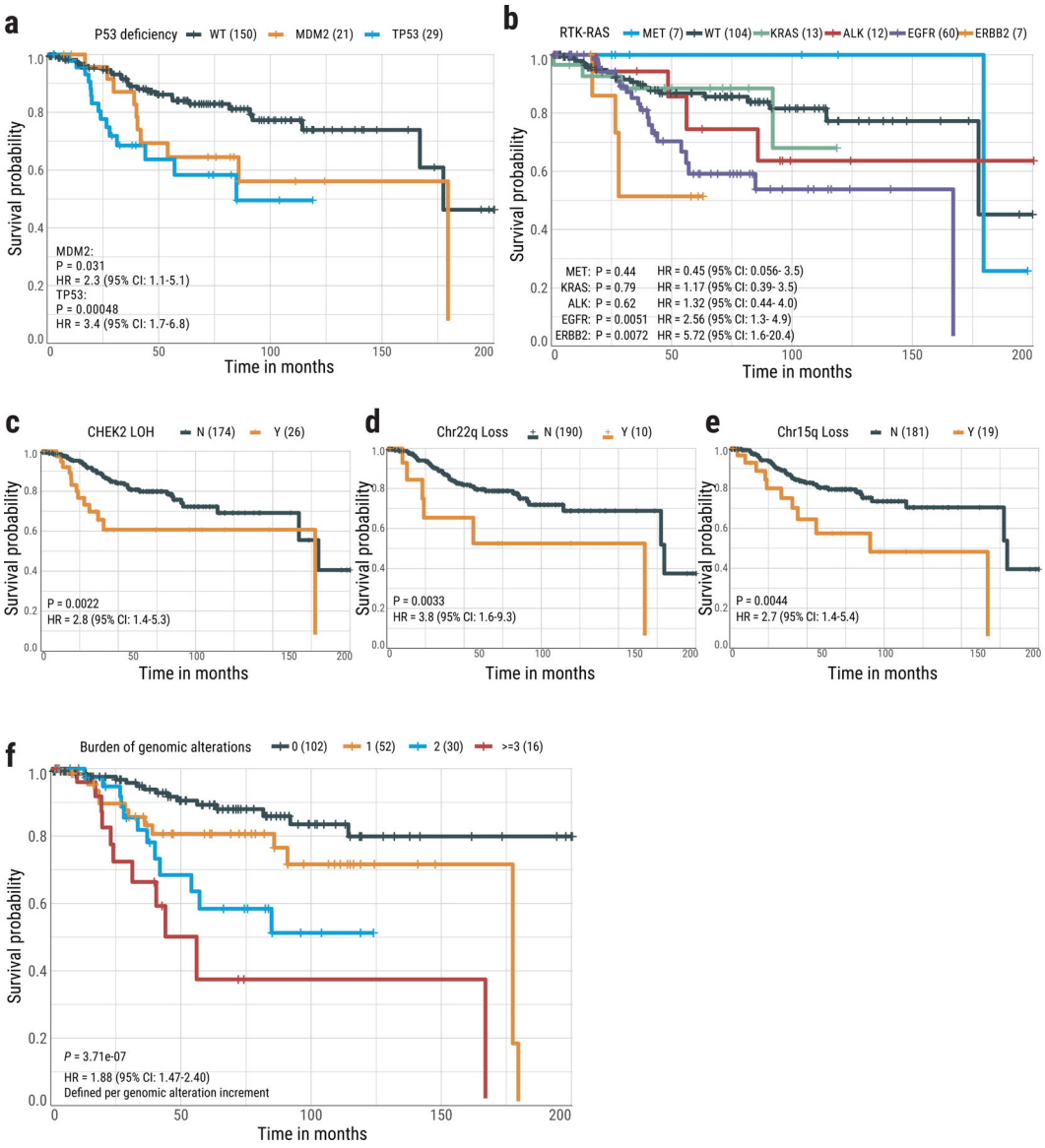

Fig. 8. Association between genomic aberrations and clinical outcomes in never smoker lung cancer patients.

Kaplan-Meier survival curves for overall survival stratified by **(a)** *TP53* mutations and *MDM2* amplification, **(b)** activation of individual driver genes in the RTK-RAS pathway, **(c)** *CHEK2* LOH, **(d)** Chr22q loss, (e) Chr15q loss, and (f) Risk score based on the burden of five genomic alterations. *P*-values for significance and hazard ratios (HR) of difference are calculated using the cox proportional hazards regression (two-sided) with adjustment for age, gender and tumor stage. No multiple-testing correction applied. For groups in each plot, Y= “with” aberration; N=“without” aberration. The numbers in brackets indicate the number of patients.